

2017-01-01

Design Of A 2000 Lbf Lox/Ich4 Throttleable Rocket Engine For A Vertical Lander

Israel Lopez

University of Texas at El Paso, israe0816@gmail.com

Follow this and additional works at: https://digitalcommons.utep.edu/open_etd



Part of the [Aerospace Engineering Commons](#), and the [Mechanical Engineering Commons](#)

Recommended Citation

Lopez, Israel, "Design Of A 2000 Lbf Lox/Ich4 Throttleable Rocket Engine For A Vertical Lander" (2017). *Open Access Theses & Dissertations*. 484.

https://digitalcommons.utep.edu/open_etd/484

This is brought to you for free and open access by DigitalCommons@UTEP. It has been accepted for inclusion in Open Access Theses & Dissertations by an authorized administrator of DigitalCommons@UTEP. For more information, please contact lweber@utep.edu.

DESIGN OF A 2000 LBF LOX/LCH₄ THROTTLEABLE ROCKET
ENGINE FOR A VERTICAL LANDER

ISRAEL LOPEZ

Master's Program in Mechanical Engineering

APPROVED:

Ahsan Choudhuri, Ph.D., Chair

Norman Love, Ph.D.

Luis Rene Contreras-Sapien, Ph.D.

Charles Ambler, Ph.D.
Dean of the Graduate School

Copyright ©

by

Israel Lopez

2017

Dedication

I would like to dedicate this thesis to my family, friends, coworkers, and all the people that supported me. I couldn't have done it without them.

DESIGN OF A 2000 LBF LOX/LCH₄ THROTTLEABLE ROCKET
ENGINE FOR A VERTICAL LANDER

by

ISRAEL LOPEZ, B.S.ME

THESIS

Presented to the Faculty of the Graduate School of

The University of Texas at El Paso

in Partial Fulfillment

of the Requirements

for the Degree of

MASTER OF SCIENCE

Department of Mechanical Engineering

THE UNIVERSITY OF TEXAS AT EL PASO

May 2017

Acknowledgements

I would first like to acknowledge Dr. Ahsan Choudhuri for giving me the opportunity to conduct research at UTEP throughout my academic career and opening many doors for a successful career. I would also like to thank Dr. Norman Love and Dr. Luis Rene Contreras for participating as members of my committee and giving their time to review my research.

A special thanks goes to Scott Hill for always providing guidance, counseling, and insight, and for ensuring that all project requirements were met. Also, special mention goes to John C. Melcher and all of the folks at Johnson Space Center for always being there to provide constant advice freely and willingly.

My sincere gratitude goes to all the people that have worked with me in this project. Their time and effort made this possible, and working with them was outstanding. Also, a thank you goes to the faculty and staff of the Mechanical Engineering Department that supported this activity.

A very special thank you goes to my friends, family, and girlfriend for always making sure that even the most stressful times were terrific. Lastly, the biggest acknowledgement goes to my parents. They have been there to support me since day one and all I accomplish I owe to them.

Abstract

Liquid oxygen (LOX) and liquid methane (LCH₄) has been recognized as an attractive rocket propellant combination because of its in-situ resource utilization (ISRU) capabilities, namely in Mars. ISRU would allow launch vehicles to carry greater payloads and promote missions to Mars. This has led to an increasing interest to develop spacecraft technologies that employ this propellant combination.

The UTEP Center for Space Exploration and Technology Research (cSETR) has focused part of its research efforts to developing LOX/LCH₄ systems. One of those projects includes the development of a vertical takeoff and landing vehicle called JANUS. This vehicle will employ a LOX/LCH₄ propulsion system. The main propulsion engine is called CROME-X and is currently being developed as part of this project. This rocket engine will employ LOX/LCH₄ propellants and is intended to operate from 2000 – 500 lbf thrust range. This thesis describes the design and development of CROME-X. Specifically, it describes the design process for the main engine components, the design criteria for each, and plans for future engine development.

Table of Contents

Acknowledgements	v
Abstract	vi
Table of Contents	vii
List of Tables	ix
List of Figures	x
Chapter 1: Introduction	1
Chapter 2: CROME-X Development Purpose	3
2.1. JANUS Robotic Lander	3
2.2. Potential future research opportunities	4
Chapter 3: Overview of Bipropellant Liquid Rocket Engines	6
Chapter 4: CROME-X Design Requirements	9
4.1. Janus' Engine Requirements	10
4.2 Engine Designated & Derived operational requirements	11
4.2.1 Mixture Ratio	12
4.2.2 Film Cooling	15
4.2.3 Chamber Pressure	15
4.2.4 Throttle Method	16
4.2.5 Nozzle Shape & Size	17
4.2.6 Component Materials	19
Chapter 5: Engine Theoretical Operation and Combustor & Nozzle Geometry	20
5.1 Rocket Performance Parameters	21
5.2 Design Process for Throttling Operation	22
5.3 MATLAB code & performance results	25
5.4 Combustor Geometry Dimensions	29
5.4.1 Diverging Nozzle Geometry	29
5.4.2 Chamber & Converging Nozzle Design	32
Chapter 6: Injector Selection and Design	36
6.1 Injection Purpose, types, and Selection Criteria	36

6.2 Pintle injection design.....	39
6.2.1 General Injector Design criteria.....	39
6.2.2 Pintle Geometry Design.....	42
6.3 Injector assembly & Testing Features.....	46
6.3.1 Testing features.....	49
6.3.1.1 Pintle Modularity.....	49
6.3.1.2 Acoustic cavity blocks	50
Chapter 7: Engine Assembly & Inlet Propellant Requirements	53
7.1 Propellant lines assembly, features, & instrumentation.....	53
7.2 Valves & Actuator Assembly	58
7.2.1 Valve selection.....	58
7.2.2 Actuator selection	61
7.2.3 V-A Connector Design	62
7.3 Inlet Propellant Requirements.....	64
7.4 Overall Engine assembly & Vehicle Interface.....	67
Chapter 8: Future Work and Conclusion	70
8.1 Component Testing & Analysis.....	70
8.1.1 Propellant seal tests.....	70
8.1.2 Valve & Actuator tests.....	71
8.1.3 Injector water tests	72
8.1.4 Pending Design & Analysis	73
8.2 Engine Hot Fire Testing.....	73
8.3 Overall Conclusions.....	74
References.....	75
Appendix.....	77
Vita	78

List of Tables

Table 4.1: Engine Requirements from JANUS.....	10
Table 4.2: Engine Designated & Derived Requirements.....	12
Table 5.1: ER and I_{sp} for Optimum Expansion for Different Thrusts	25
Table 5.2: Engine Parameters for Optimal Expansion at 1250 lbf Thrust.....	27
Table 5.3: Cone Nozzle vs Bell Nozzle Geometries.....	31
Table 6.1: Propellant Properties & Injection Parameters.....	41
Table 7.1: Main Engine Valve Requirements.....	59
Table 7.2: Valve Actuator Requirements.....	61
Table 7.3: Propellant Required Conditions Downstream of Injection.....	64
Table 7.4: Overview of the Propellant Delivery Line Losses.....	66
Table 7.5: Engine Required Inlet Propellant Conditions	67
Table 8.1: Preliminary Test Plan	74

List of Figures

Figure 2.1: JANUS Vehicle and Flight Profile	4
Figure 2.2: Regenerative & Film Cooling [4]	5
Figure 3.1: Rocket Engine Chamber and Nozzle Configuration [2]	7
Figure 4.1: Optimum MR vs. P_c for LOX/LCH ₄ Propellants	13
Figure 4.2: Combustion Temperature (T_c) vs. MR for different P_c values	14
Figure 4.3: Sea Level I_{sp} vs. MR for different P_c values	14
Figure 4.4: Under-expansion, Over-expansion, and Optimum Expansion [1]	18
Figure 5.1: Expected Chamber Pressure & Weight Flow rate vs. Thrust	28
Figure 5.2: Engine I_{sp} vs. Thrust	29
Figure 5.3: Conical Nozzle Shape [5]	30
Figure 5.4: Bell Nozzle Contour [5]	31
Figure 5.5: Comparison of Cone Nozzle vs Bell Nozzle for CROME-X	32
Figure 5.6: Dimensions of the Combustion Chamber and Nozzle	34
Figure 5.7: Chamber and Nozzle for CROME-X	35
Figure 6.1: Different Injector Configurations [1]	37
Figure 6.2: Injection Spray of a Pintle Injector (Annular, Radial, and Combined Flow) [19]	38
Figure 6.3: dP/P_c vs Thrust for the Injection Areas	42
Figure 6.4: Pintle Injection Jets and Spray Angle [21]	43
Figure 6.5: Pintle Injector Dimensions [21]	44
Figure 6.6: Pintle Primary and Secondary Radial Holes [21]	45
Figure 6.7: CROME-X Pintle Post Radial Orifices	45
Figure 6.8: Pintle Injector Cross Section View	47
Figure 6.9: Pintle Injector Assembly Exploded View	47
Figure 6.10: Pintle Injector Bottom View	48
Figure 6.11: Combustion Instability Types and Description [1]	50
Figure 6.12: Dog-leg Cavities With and Without Acoustic Cavity Blocks	51
Figure 6.13: Acoustic Cavity Blocks of Different Size	52
Figure 7.1: Quick-Clamp Sanitary Tube Fittings and Components [27]	55
Figure 7.2: Propellant Feed Line Assembly	55
Figure 7.3: Propellant Feed Line Assembly Top View	56
Figure 7.4: Injector Instrument Stand	57
Figure 7.5: Instrumentation Ring Location & Cross Section View	58
Figure 7.6: Ball Valve V-ports vs. Round Port (30°, 60°, 90° and round port)	59
Figure 7.7: Main Engine Valves – 60° V-port Control Valve	60
Figure 7.8: Actuator DC Motor (left) and Gearbox (right)	61
Figure 7.9: V-A Connector & Thermal Contour for Expected Thermal Gradient	63
Figure 7.10: Valve-Actuator Assembly	63
Figure 7.11: Full CROME-X Assembly and Dimensions	68
Figure 7.12: CROME-X with the Vehicle Interface	69
Figure 7.13: Engine Module Attached to the JANUS Load Cell Module	69
Figure 8.1: Engine Flanges That Employ Gore Seal	71
Figure 8.2: Gore Seal Test Article and Configuration	71
Figure 8.3: Injector Water Test Setup	72

Chapter 1: Introduction

Recent interest has been placed on liquid oxygen (LOX) and liquid methane (LCH₄) for rocket propulsion applications. Historically, better performing propellant combinations have been employed, like liquid hydrogen and LOX. However, LOX and LCH₄ offer several advantages as a rocket propellant combination. These advantages include lower toxicity than other propellants (like hydrazine) and easier handling and storage compared to other cryogenics (like liquid hydrogen) [1]. Additionally, the greatest advantage this propellant combination offers is the potential to be harvested in the surface of Mars. This is known as in-situ resource utilization (ISRU). ISRU would enable the production of propellants off-planet and help reduce the weight of launch vehicles, allowing greater launch payloads [2]. This makes LOX/LCH₄ an attractive propellant choice given the recent interest in Mars exploration missions.

Surprisingly, there is no history of LOX/LCH₄ spaceflight engines [1]. This has led companies and organizations to push forward with the development of LOX/LCH₄ technologies. Examples from the private sector include the SpaceX Raptor engine, which will be used for Mars colonizing vehicles, and the Blue Origin BE-4 engine, intended for use on their orbital launch vehicles. Other examples include NASA's Project Morpheus, which developed a lander capable of vertical takeoff and landing propelled by a LOX/LCH₄ engine [3].

The CROME-X Engine is a project intended to develop a 2000 lbf rocket engine that uses a LOX/LCH₄ propellant combination. This project is being carried out at the Center for Space Exploration and Technology Research (cSETR). CROME-X will be the main propulsion system for JANUS, a robotic lander vehicle. The end goal of JANUS and CROME-X is to demonstrate successful operation of integrated LOX/LCH₄ technologies. Since the vehicle will perform controlled takeoff and landing maneuvers, the vehicle requires the engine to be throttleable. The required range of operation is 2000 – 500 lbf thrust. Once fabricated, JANUS and CROME-X tests will occur at the UTEP Technology Research and Innovation Acceleration Park (tRIAC). This test facility is located in Fabens, TX, and construction is overseen by cSETR.

This paper focuses on the design process used to develop the first version of CROME-X. The initial chapter discusses the project requirements for the engine. The subsequent chapters include a description of how some engine components were designed or selected. The paper concludes with a description of component tests to be conducted before engine fabrication, and a preliminary test plan for engine hot fire testing.

Chapter 2: CROME-X Development Purpose

The CROME-X engine will be employed as the main propulsion engine for the JANUS robotic lander vehicle. Both the vehicle and the engine are being developed in parallel, so many of the engine requirements are derived from JANUS. Moreover, future versions of CROME-X will be used as an opportunity to implement active use of regenerative cooling, as well as additive manufacturing for engine components.

2.1. JANUS ROBOTIC LANDER

JANUS is a robotic lander vehicle that serves as a methane propulsion technology testbed. This vehicle is currently being developed at the cSETR. The goal of the JANUS project involves demonstrating a flight-capable vehicle that incorporates various methane propulsion technologies into a fully operational autonomous integrated system. The propulsion system includes the main engine and a reaction control system (RCS). Other systems include: the propellant delivery system; guidance, navigation, and control; and the vehicle main structure.

The vehicle configuration is a vertical structure surrounding three tanks (two propellant tanks and a pressurizing gas tank). The pressurization system will be blowdown, so there is no external pressure source and the system pressure is allowed to decay as the propellant is used [4]. The main engine will be attached to the bottom of the vehicle through a gimbal, while the RCS engines will be placed laterally midways of the structure. The vehicle flight mission comprises a non-tethered flight demonstration that successfully conducts a takeoff, midair hover and roll, and soft landing under full autonomous system control. The vehicle is expected to remain in low altitude when hovering (20 ft., nominal). The full mission (takeoff to landing) is estimated to last for about 30-40 seconds. Roll maneuvers will be conducted using 5 lbf RCS engines (i.e. the cSETR Pencil Thruster). Main vehicle maneuvers and dynamic control will be carried through the main engine gimbal. Because of this reason, the CROME-X engine will have to throttle over the vehicle's necessary thrust range. A picture of JANUS conceptual design and its flight profile can be seen in Figure 2.1.

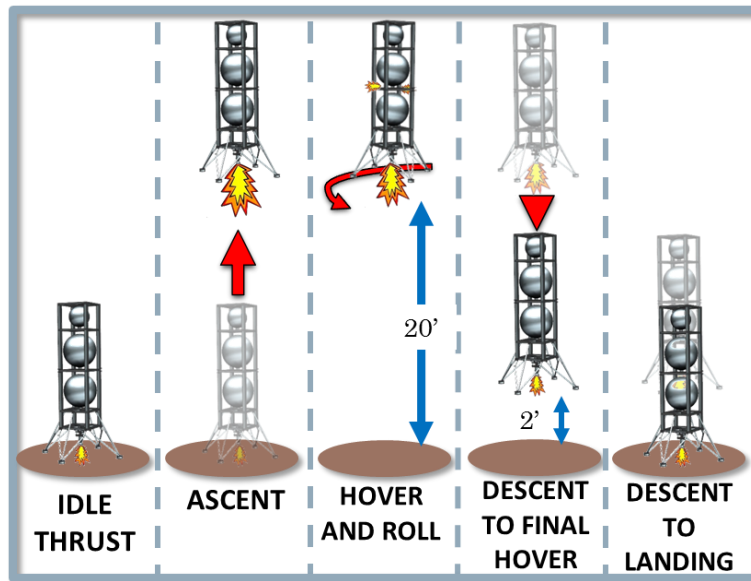


Figure 2.1: JANUS Vehicle and Flight Profile

2.2. POTENTIAL FUTURE RESEARCH OPPORTUNITIES

Regenerative cooling is a cooling method where a liquid propellant is fed through passages in the chamber wall and circulates thorough the passages to keep the chamber cool. The propellant is then fed into the injector before being injected into the chamber for combustion.

Regenerative cooling offers several advantages vs. other liquid cooling methods (such as film cooling). For example, film cooling uses liquid propellant that is injected towards the combustion wall, forming a film that keeps the wall cool. As the film travels downstream the propellant is gasified. Thus the propellant is expended. In contrast, regenerative cooling employs just the combustion liquid propellant for cooling. Because no propellant is wasted, regenerative cooling improves engine performance. Moreover, the heat absorbed by the coolant is not wasted and the increase of energy content leads to a slight increase in performance as well [5] [1]. This two cooling methods can be seen in Figure 2.2. Because methane engine development for flight vehicles has been limited, there is the opportunity to explore the feasibility of producing regenerative cooled engines using a LOX/LCH₄ propellant combination. The current CROME-X

engine design will use fuel film cooling (FFC) due to its relative design simplicity, but future versions of the engine will attempt to implement a regenerative cooling design.

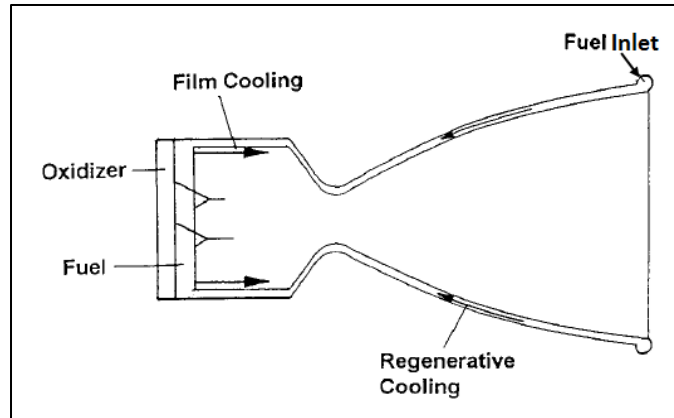


Figure 2.2: Regenerative & Film Cooling [4]

Additive manufacturing is a fast growing technology that is now being explored for use in space flight applications [6]. Rocket engine components are usually complex in design, take long fabrication times, and are costly to manufacture using conventional manufacturing techniques. Additive manufacturing has the potential to overcome those disadvantages by offering reduced cost, faster fabrication times, and design flexibility not limited by conventional manufacturing [7]. Certainly, the additive process still faces challenges that inhibit extended use for component fabrication (e.g. rough surface finish, porosity, etc.). Nevertheless, as the technology improves, additive manufacturing could provide a significant advantage for rocket engine design [6]. Consequently, future versions of the CROME-X engine will explore how to successfully incorporate components that are created using additive manufacturing.

Chapter 3: Overview of Bipropellant Liquid Rocket Engines

Rocket engines generate thrust by ejecting high velocity matter, producing a force in the opposite direction of flow [5]. This matter is normally high pressure & high temperature gas produced in a cylindrical combustion chamber that accelerates to supersonic velocities through a de Laval nozzle (converging-diverging nozzle). A conventional engine configuration is shown in Figure 3.1. The converging nozzle section accelerates the gas until it reaches the throat (i.e. the smallest cross sectional area of the nozzle). Because of compressible flow effects, the gas reaches sonic velocity (Mach 1) at the throat, the maximum velocity attainable with a converging nozzle. Once the flow is sonic, increasing the flow area further increases gas velocity. Therefore a diverging nozzle is used to achieve supersonic velocities. The gas velocity increases at the expense of pressure, so the pressure decays as velocity increases throughout the length of the nozzle [4]. The thrust generated by this process can be summarized by the thrust equation as shown below.

$$F = \dot{m}v_e + (P_e - P_a)A_e \quad (3.1)$$

Here the F stands for thrust, \dot{m} for mass flow rate, v_e is the exit velocity of the gas, P_e and P_a are the exit and ambient static pressure, and A_e is the area of the nozzle exit. The equation is composed of the sum of two thrust components. The first component of the equation is the thrust generated by the momentum exchange of the fluid. The second component is the thrust generated by the pressure imbalance at the exit of the nozzle [4]. Thus, it can be seen that thrust is higher in vacuum because the ambient pressure is practically zero. For engines that operate in the atmosphere, it is ideal to have the exit pressure equal the ambient pressure ($P_e = P_a$). This condition is called optimal expansion, and provides the maximum performance for atmospheric engines [4].

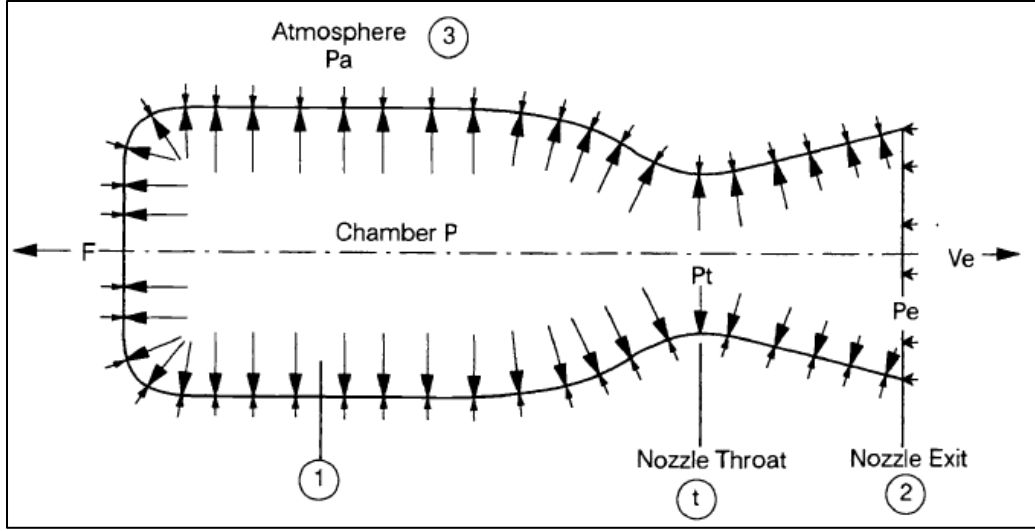


Figure 3.1: Rocket Engine Chamber and Nozzle Configuration [2]

In order for the flow to reach sonic conditions, the ratio between the exit pressure and the chamber pressure has to be lower than the critical pressure ratio. The critical pressure ratio is defined by Eqn. 3.2.

$$\frac{P_t}{P_c} = \left(\frac{2}{k+1} \right)^{\frac{k}{k-1}} \quad (3.2)$$

Here P_t is the pressure at the throat, P_c is the chamber total pressure at the nozzle inlet, and k is the specific heat ratio of the gas. The critical pressure ratio is specific to a gas composition because it depends on the specific heat value only. If the pressure ratio between P_e and P_c is greater than the critical pressure ratio, the flow will not reach sonic conditions and the divergent nozzle will slow down the gas instead of increase the velocity [1]. From thermodynamics, the theoretical exit velocity of a gas can be expressed as follows.

$$v_e = \sqrt{\frac{2kgRT_c}{k-1} \left[1 - \left(\frac{P_e}{P_c} \right)^{\frac{k-1}{k}} \right]} \quad (3.3)$$

In this equation R is the specific gas constant of the exhaust gas (or combustion products), T_c is the chamber total temperature, and g is the gravitational constant. From this equation it is evident that increasing the gas temperature, increasing chamber pressure, and/or decreasing the exit pressure will lead to higher exit velocity (and thus higher thrust) [4].

Another important performance indicator for rocket engines is called the specific impulse (I_{sp}), which is defined by the following equation.

$$I_{sp} = \frac{F}{\dot{m}g} \quad (3.4)$$

Specific impulse indicates how much impulse can be imparted to a vehicle for a given amount of propellant used [8]. Therefore it allows a performance comparison of different engine types and configurations. It can be seen that decreasing the mass flow rate consumption yields an increase in performance.

Bipropellant rocket engines follow all the principles described but have distinctive characteristics. Specifically, a bipropellant engine generates gas through combustion of two liquid propellants; an oxidizer and a fuel. The propellants are fed into the engine chamber through an injector, delivering the propellants at the necessary proportions and conditions to achieve combustion [5]. The proportion of the propellants is called the mixture ratio (MR), which is defined as the ratio of the oxidizer to fuel mass flow rates (Eqn. 3.5).

$$MR = \frac{\dot{m}_{ox}}{\dot{m}_f} \quad (3.5)$$

The MR and T_c are directly related for a specific propellant combination. Increasing the mixture ratio leads to an increase in combustion temperature. The temperature reaches a maximum at stoichiometric MR conditions and then decrease as the MR further increases. Although theoretically the maximum temperature is achieved at stoichiometric MR, propellant combinations usually have an optimum MR that delivers the maximum energy release, thus producing maximum I_{sp} [4]. The optimum MR is generally more fuel rich (i.e. smaller than stoichiometric MR) and thus yields a lower flame temperature than stoichiometric conditions [5].

From the theoretical relationships described, it is evident that the performance of a bipropellant engine will depend on specific system parameters. These include the propellant combination, MR, chamber pressure, and atmospheric conditions for operation. These parameters will be discussed more in detail in the following chapters.

Chapter 4: CROME-X Design Requirements

The development of the JANUS vehicle and the CROME-X engine is being carried out in parallel. The mission objectives and functional requirements take precedence and become design drivers for the overall system. These requirements lead to the breakdown of specific requirements for each subsystem (e.g. the vehicle structure, engine, or propellant delivery system). Because there is no one solution to meet the mission objectives, the subsystem requirements go through an iterative tradeoff process that satisfy the overall objectives. Thus, individual subsystem requirements are intimately related; any parameter change to one will fundamentally affect the other [9].

As the design process evolved, iterations and tradeoffs were conducted to satisfy the mission requirements. This mainly involved the compromise of vehicle and engine requirements. For example, selecting a cryogenic propellant requires tanks made of a compatible material and insulation. A specific propellant combination delimits engine performance and its minimum propellant consumption. The propellant consumption will define the propellant necessary for any given mission/maneuver; the amount of necessary propellant defines the size and amount of tanks. The engine MR dictates the proportion of oxidizer to fuel, consequently affecting the relative size between each tank [4]. Because the system is blowdown, the maximum system pressure will limit the engine chamber pressure, limiting the engine performance and size. Engine flow rates and pressure requirements will determine feed line size and length. Furthermore, the vehicle structure will have to support all these components and will either control or adapt to different vehicle constraints and configurations.

Because the effect of a subsystem requirement affects others, careful consideration for the vehicle and engine requirements was taken when formulizing their definition. Because this project focuses on the engine development, the requirements discussed involve those for the engine only. Specifically, this requirements can be divided in two. The first set includes the requirements dictated by the vehicle for the engine. The second set are the engine requirements imposed for the

vehicle. In turn, integrating both of these subsystem requirements led to a set of derived engine design requirements. The following sections first show the vehicle requirements for the engine, and then the engine designated & derived requirements. These sections describe in detail their values and reason for selection.

4.1. JANUS' ENGINE REQUIREMENTS

In order to achieve its mission successfully, the JANUS vehicle decreed a set of engine requirements. These requirements are shown in Table 4.1, and will be discussed in detail in the next paragraphs.

Table 4.1: Engine Requirements from JANUS

Requirement	Value
Thrust	500 – 2000 lbf
Operation / Ambient Pressure	Steady-state / $P_a = 12.8$ psia
Propellants	LOX/LCH ₄
Min System I_{sp}	145 seconds @ 2000 lbf thrust
Max Tank Pressure	400 psia
Max Envelope Size (cylindrical)	≤ 2.5 ft (diameter) x 4 ft (long)

Different thrust levels are required to have vehicle dynamic control. Therefore the CROME-X engine requires by principle to be a throttleable engine. Based on vehicle conceptual size and weight, the vehicle thrust requirement was defined to be 2000 lbf with a 4:1 throttle ratio. Thus, the engine will have to generate successfully 2000 lbf max thrust down to 500 lbf. Moreover, the engine will operate in steady state mode; namely, be able to deliver steady thrust indefinitely while there is propellant (this is in contrast to pulsing engines, which are intended to generate short bursts of thrust for precise impulse delivery) [4]. During flight the vehicle will remain at low altitude, so the engine is considered a sea level engine. The optimum expansion ambient pressure employed will be from the tRIAC test site in Fabens, TX ($P_a \approx 12.8$ psia).

As previously stated, the propellants will be liquid oxygen (LOX) and liquid methane (LCH₄). Being cryogenic propellants, the saturation temperature of LOX & LCH₄ is around -300 and -260 °F at ambient pressure. As a result all components of the engine should be able to withstand these temperatures. Furthermore, LOX is incompatible with many materials, so careful consideration with material selection is important.

Unlike combustion I_{sp} , system I_{sp} includes any cooling or extra propellant used aside from combustion. Throughout this document, unless otherwise specified, mentioning I_{sp} implies the combustion I_{sp} . Since the vehicle has limited propellant capacity, the vehicle requires a minimum system specific impulse of 145 seconds at maximum thrust. The 145 seconds correspond to using the total tank propellant capacity while running the engine at 2000 lbf for 40 seconds. Furthermore, the tanks will have a maximum operating pressure of 400 psia. This quantity does not include feed line pressure losses before the propellant reaches the engine, so the engine requires a lower operating pressure. Lastly, the vehicle will be limited in size, so the maximum envelope size for the engine assembly will be a cylindrical geometry of 2.5 ft in diameter and 4 ft long.

4.2 ENGINE DESIGNATED & DERIVED OPERATIONAL REQUIREMENTS

The section describes the requirements for the engine to provide the thrust and performance requirements discussed previously. These include both chosen and derived quantities. These values are shown in Table 4.2, and are further discussed in the next passages. Several calculations and quantities used to compare rocket characteristics and performance were computed using the NASA CEA (Chemical Equilibrium with Applications) and RPA (Rocket Propulsion Analysis) software. CEA is a computer program that calculates chemical equilibrium compositions (including combustion of different propellants), and RPA is an analysis software tool that computes theoretical rocket engine performance and design calculations [10] [11]. Also, some propellant fluid properties were obtained using REFPROP, a NIST database with fluid thermodynamic and transport properties [12].

Table 4.2: Engine Designated & Derived Requirements

Requirement	Value
Mixture Ratio (MR)	Combustion: 2.7 System: 1.89
Fuel Film Cooling (FFC)	$\leq 30\%$ of Fuel Flow
Chamber Pressure (P_c)	232.8 – 75.2 psia
Throttle Method	Main Valve Actuation
Expansion Ratio (ER) & Nozzle Shape	ER: 2.7 Conical (15°)
Component Materials	Chamber & Nozzle: Inconel 718 Injector: Inconel 625 Manifolds and lines: SS 316

4.2.1 Mixture Ratio

The combustion MR for the engine was defined by first finding the optimum MR of LOX/LCH₄ at different chamber pressures. Figure 4.1: shows a chart with these values. This chart was generated using both CEA and RPA. The curve in the chart is not smooth due to rounding errors of decimal places in the results; the results are deemed acceptable for comparison nonetheless. From the chart it can be seen that the optimal MR range varies somewhere around 2.7 to 3.1 (up to pressures of 400 psia).

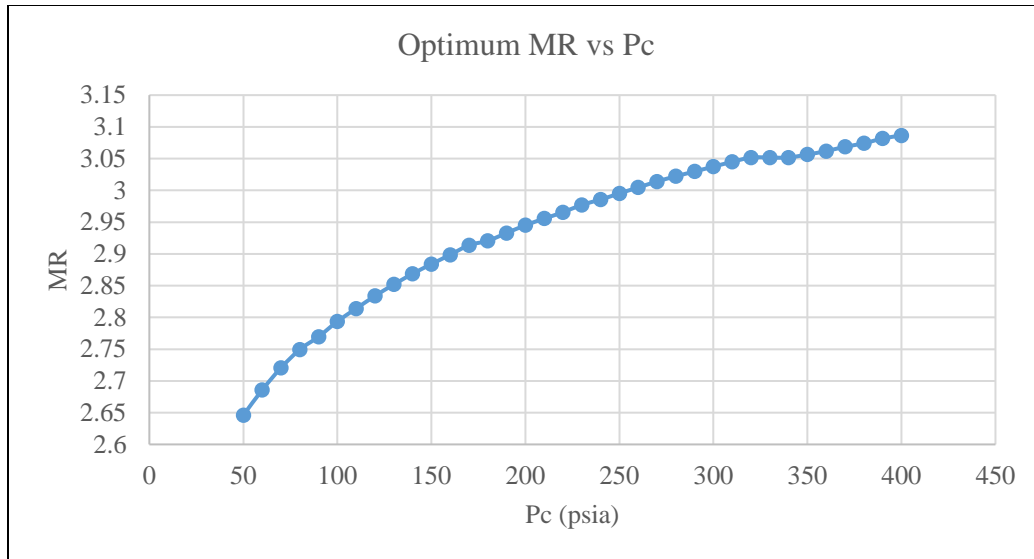


Figure 4.1: Optimum MR vs. P_c for LOX/LCH₄ Propellants

After assessing the data, an MR of 2.7 was selected. Although a higher MR would theoretically provide higher performance, there are several reasons why an MR of 2.7 would prove beneficial. First, at mentioned pressures and saturation temperature of LOX & LCH₄, a ratio of 2.7 leads to equal tank size. This occurs because at those conditions the density of liquid oxygen is approximately 2.7 times greater than the density of liquid methane, leading to equal propellant volume. Equal tank size reduces vehicle complexity because tank design can be similar for both propellants. Second, a higher MR leads to higher combustion temperatures, requiring more cooling. Figure 4.2 demonstrates T_c for different MRs at different combustion pressures. The data illustrates that combustion temperature is more dependent on MR than pressure, and reducing the MR from 3.1 to 2.7 can reduce the max temperature by up to 200°R for a given pressure. Additionally, decreasing the MR to 2.7 does not exceedingly impact performance. Figure 4.3 shows the theoretical sea level I_{sp} for different MR values. For any shown pressure the performance drops by less than 3 seconds, being relatively low compared to the total I_{sp} estimates (around 246 – 269 seconds). This drop in temperature was deemed acceptable at the expense of the low performance drop.

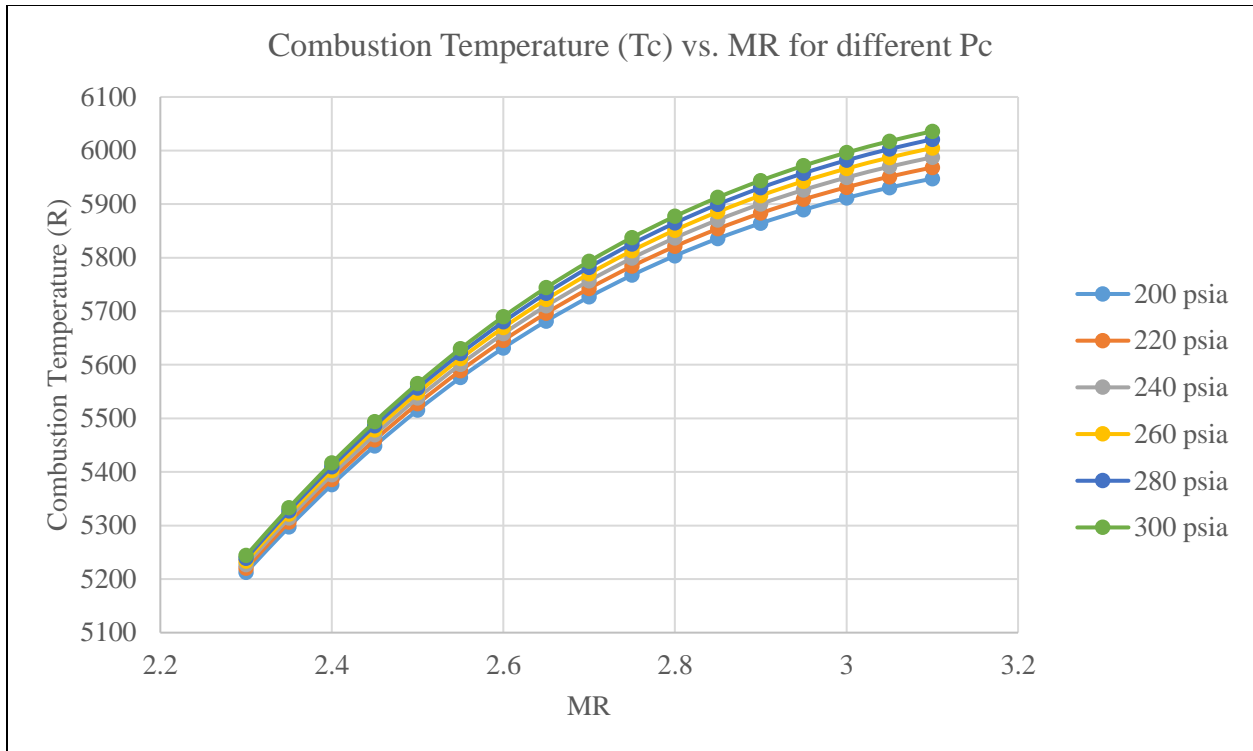


Figure 4.2: Combustion Temperature (T_c) vs. MR for different P_c values

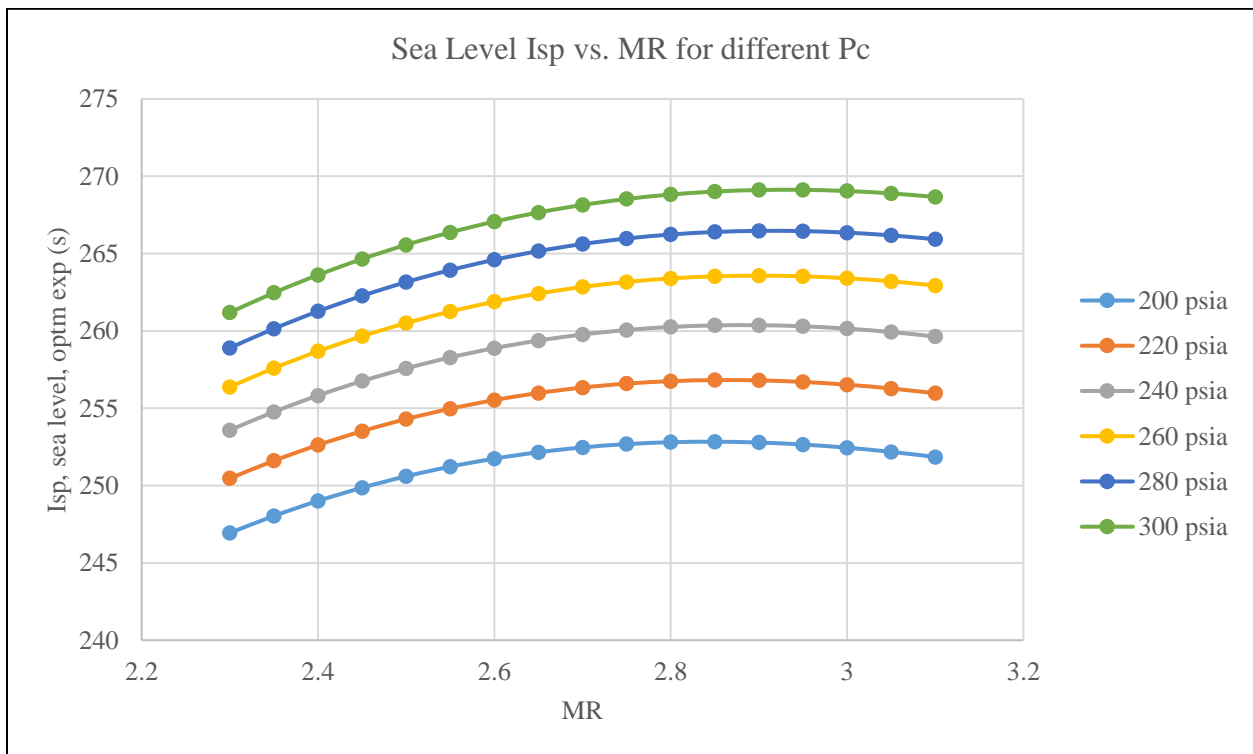


Figure 4.3: Sea Level I_{sp} vs. MR for different P_c values

4.2.2 Film Cooling

Since the expected combustion temperatures are hotter than any conventional material could withstand ($> 5000^{\circ}\text{R}$), cooling is necessary for steady state operation. As previously stated, the engine will use fuel film cooling (FFC). Because this cooling method employs extra expendable propellant, it reduces engine performance because more propellant is used for operation [1]. Nonetheless, this loss in performance is considered acceptable for the first version of this engine. Extra fuel (LCH_4) will be used to cool the engine, and a lower MR will result for the overall engine system. Thus, two MRs are considered for engine operation: the combustion MR (only considers propellant used for combustion) and a system MR (takes into account all propellant flow rate; combustion and cooling propellant). Throughout this document, unless otherwise specified, mentioning MR implies the combustion MR.

Previous tests with LOX/LCH_4 engines of similar size & material have shown that around 30% of the total fuel propellant is more than necessary to cool the engine effectively with FFC [13]. Therefore, the engine will be designed to provide a maximum of 30% FFC. Engine testing will be conducted to determine the optimum amount of FFC (potentially lower than 30%). Adjusting for extra fuel flow yields a system MR of 1.89, assuming that the fuel flow necessary for combustion will be 70%. Certainly, there was mention that an MR of 2.7 was selected to allow the vehicle an equal tank configuration. Regardless, the first version of CROME-X will be for development purposes only, and a system MR of 1.89 is expected for testing of the first engine. Future engine models (e.g. the vehicle flight engine) will employ regenerative cooling, preventing the extra fuel loss and maintain a system MR of 2.7.

4.2.3 Chamber Pressure

The engine chamber pressure was selected as a compromise between the vehicle allowable system pressure (400 psia) and the expected performance of the engine. As previously stated, pressure losses are expected throughout the propellant delivery system of the vehicle. Furthermore, inlet valve losses are unavoidable and injector pressure losses are necessary to improve propellant

atomization and prevent unstable combustion pressure oscillations [5]. Consequently, the P_c value has to be lower than the tank pressure to allow some margin for these losses. Nevertheless, maintaining a high chamber pressure is desirable because higher P_c values lead to greater engine performance (as seen in Figure 4.3). For this reason, an operating P_c of 232.8 psia at maximum thrust was selected. This pressure theoretically produces a specific impulse greater than the vehicle required minimum I_{sp} (≈ 250 vs. 145 seconds), potentially reducing the necessary amount of propellant. Furthermore, that chamber pressure permits a substantial amount of pressure drop between the combustion chamber and the tanks. Injector pressure drop levels close to 30% of total chamber pressure have been observed in similar stable throttleable engines [14]. Using that assumption, the injector pressure drop could potentially be around 70 psi ($\approx 30\%$ of 232.8 psia). As a result, the engine would need around 300 psia upstream of the injector, allowing ample room for pressure losses in the line and valves. The number 232.8 psia was chosen for convenience; the ambient pressure is around 12.8 psia, allowing gage pressure readings at 220 psig. The low end thrust chamber pressure (75.2 psia) was computed using a process shown in chapter 5.

4.2.4 Throttle Method

Throttling an engine requires a mechanism that alters the flow rate, resulting in thrust output variations. Historically, rocket engines have achieved this by either restricting the flow upstream of the injector (e.g. throttle valve), or by employing an injector with adjustable components that change the injection area (and thus change the flow). Selecting a method usually depends on the required throttle level and the desired injector complexity. An important aspect of throttling is injector pressure drop, usually denoted as a percentage of total chamber pressure (or dP/P_c). A nominal level of approximately 20% dP/P_c is usually necessary to maintain stable combustion [1]. Employing a valve to regulate the flow generally reduces the throttle range because the injector pressure drop is non-linear. Thrust and P_c change approximately proportional with flow, whereas injector pressure drop changes as the square of the flowrate. Subsequently, low thrust levels reduce the dP/P_c to much lower levels, potentially introducing instabilities [5]. In

contrast, an injector with movable components is more apt for deep throttle levels because the dP/P_c can be controlled more effectively, but designing such injector is generally a more complex and difficult task. To reduce design complexity, CROME-X will be throttled using independently actuated valves. Independent actuating will permit control of the MR if necessary.

4.2.5 Nozzle Shape & Size

As mentioned previously, a rocket engine employs a converging-diverging nozzle to increase the exit velocity of the gases. Moreover, the gas exit pressure affects thrust output and performance. For a given chamber pressure, the exit pressure depends on the nozzle expansion ratio (ER), which is the ratio of the nozzle exit area to the throat area. This relationship can be defined from thermodynamics as illustrated on Eqn. 4.1.

$$ER = \frac{A_e}{A_t} = \frac{\sqrt{k \left(\frac{2}{k+1} \right)^{\frac{k+1}{k-1}}}}{\left(\frac{P_e}{P_c} \right)^{\frac{1}{k}} \sqrt{\frac{2k}{k-1} \left[1 - \left(\frac{P_e}{P_c} \right)^{\frac{k-1}{k}} \right]}} \quad (4.1)$$

The expansion ratio represents an actual geometrical feature of the engine and the value is fixed depending on the designated nozzle size. Moreover, to produce maximum performance the expansion ratio has to deliver optimum expansion ($P_e = P_a$). Producing optimum expansion becomes problematic for throttleable engines. Even though the altitude of the vehicle will be relatively low (and ambient pressure will remain fairly constant), the chamber pressure will change for different throttle levels, resulting in different exit pressures for a fixed expansion ratio [1]. Exit pressures different than ambient result in two nozzle conditions: under-expanded and over-expanded (Figure 4.4). An under-expanded nozzle discharges gas at higher pressure than ambient pressure ($P_e > P_a$). This results in an expansion wave at the nozzle exit, leading to lower performance due to incomplete expansion inside the nozzle and wasting potential velocity increase. In contrast, an over-expanded nozzle discharges gas at a lower pressure than ambient pressure ($P_e < P_a$). This also leads to performance loss due to inefficient expansion, and if the exit pressure is severely lower than ambient it could result in flow separation from the nozzle wall.

Uneven flow separation can produce nozzle side loads that are potentially destructive. As a result, gross over-expansion is highly undesirable [1].

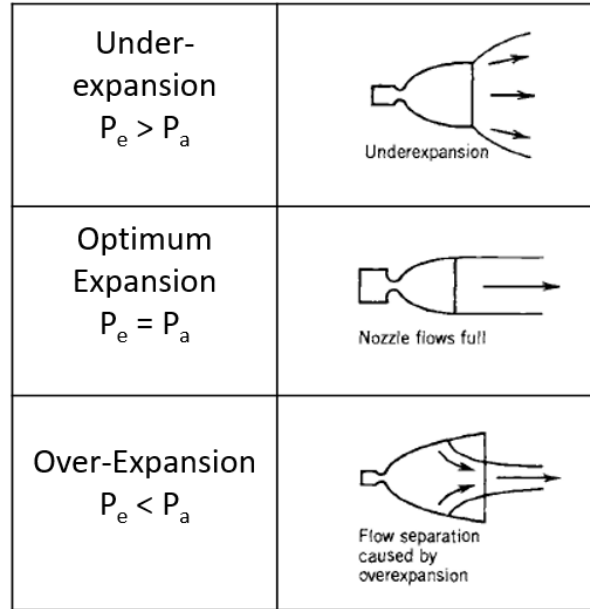


Figure 4.4: Under-expansion, Over-expansion, and Optimum Expansion [1]

Choosing an expansion ratio with optimum expansion at 2000 lbf thrust would result in substantial over-expansion at low end thrust (500 lbf). Conversely, selecting an expansion ratio for optimum expansion at 500 lbf results in a highly under-expanded nozzle at high end thrust. Because both situations lead to low performance, an expansion ratio between both cases was selected. This compromise would lead to acceptable performance losses at high end thrust but prevent unstable over-expansion at low end thrust. The engine expansion ratio was designated to be 2.7, corresponding to an optimum expansion expected to occur at 1250 lbf thrust (and $P_e \approx 154$ psia). The method used to compute these values will be shown in chapter 5. Moreover, the nozzle shape was chosen to be a conical nozzle with a 15° half-angle. Most atmospheric rocket engines usually employ a bell shape nozzle, resulting in a shorter nozzle and better efficiency, but also greater fabrication difficulty due to its contoured shape [5]. The increase in performance holds true for expansion ratios greater than 5 (with ER values up to 50). Because the CROME-X expansion

ratio is significantly small ($ER = 2.7$), a conical nozzle is essentially of similar shape and size compared to a bell nozzle. The ease of fabricating a cone nozzle corroborates the decision to use a conical nozzle. A more detailed assessment will be shown in chapter 5.

4.2.6 Component Materials

The engine will be exposed to different temperature and mechanical loading conditions. Specifically, it will be exposed to both cryogenic and hot temperature conditions at high pressures. Inconel 718 & 625 (nickel-chrome super alloys) were chosen as the material for the combustor and injector, respectively, and stainless steel 316 for the propellant feed lines going into the injector. All three metals are compatible with LOX & LCH₄, can be used in cryogenic applications, and can be welded to each other. [15] Additionally, Inconel alloys are generally used in aerospace applications, and alloys 718 & 625 can be used for additive manufacturing making 3D printed components an attractive and viable option. Inconel 718 has great corrosion, oxidation, & creep resistance, and relatively high melting temperature range (2300 – 2437 °F). Moreover, its good strength properties at high temperature make it a viable choice for the combustor body (chamber & nozzle) [16]. The maximum Inconel 718 temperature that will be allowed is 2000°F during steady state operation to keep a 300 degree gap from its melting range. Inconel 625 offers equivalent properties and melting temperature range to Inconel 718. However, Inconel 718 is stronger than Inconel 625 (for example, a 180 vs 120 ksi ultimate strength at room temperature, respectively). Due to its higher strength, alloy 718 is harder to machine than 625 [17]. Because injector geometries are usually more intricate to fabricate, ease of machinability makes alloy 625 a more reasonable choice for the injector. Stainless steel 316 was selected for the propellant feed lines because it is a conventional material for tubing & fittings, and a less expensive option compared to the other super alloys.

Chapter 5: Engine Theoretical Operation and Combustor & Nozzle Geometry

Engine performance can be divided in two: the propellant combustion performance and the nozzle's ability to expand the combustion gases [5]. These two performance indicators are called characteristic velocity and thrust coefficient, respectively. Both are theoretically quantifiable for a given propellant combination and the engine geometrical characteristics. To calculate these values it is first necessary to identify the combustion products and their intensive properties. These can next be used to establish the geometry of the combustion chamber and the de Laval nozzle. From this results, one can determine the engine operating parameters for a desired thrust output (e.g. propellant pressures, flow rates, specific impulse, etc.). However, throttling an engine alters the combustion process at different thrust levels, requiring an assessment of the combustion performance for different conditions.

The following sections discuss the method used generate the mentioned performance indicators, the engine operating parameters, and the design of the chamber and nozzle. The theoretical equations used are derived from compressible flow assumptions. Rocket chamber and nozzle design follows the same assumptions. These assumptions are listed below [5].

- Homogenous gas composition
- Perfect gas
- No heat transfer through walls (i.e. adiabatic)
- No friction
- Steady flowrate
- One-dimensional flow
- Uniform velocity across any section normal to the chamber axis
- Chemical equilibrium within the combustion chamber and constant throughout the nozzle

5.1 ROCKET PERFORMANCE PARAMETERS

For a given propellant combination there is theoretical maximum energy output. Characteristic velocity (C^*) is a rocket parameter used to compare the thermochemical combustion performance of any propellant combination [4]. The C^* value indicates how many pounds of propellant need to be combusted to maintain a certain pressure. This parameter is defined in Eqn. 5.1.

$$C^* = \frac{P_c A_t g}{\dot{w}} = \frac{\sqrt{k g R T_c}}{k \sqrt{\left(\frac{2}{k+1}\right)^{\frac{k+1}{k-1}}}} \quad (5.1)$$

In this equation, \dot{w} is the propellant weight flow rate ($\dot{w} = \dot{m}g$), and A_t is the area of the throat [4]. The left side of the equation is the empirical method of calculating the C^* value. The right side of the equation shows that C^* is theoretically a propellant property. The units of C^* are length over time (for example, ft/s), hence it is dubbed as a “velocity”. Propellant combinations with higher theoretical C^* values are better performing because they require less propellant.

Thrust coefficient (C_F) is a non-dimensional quantity used to quantify how much thrust is augmented by the diverging section of the nozzle. This value is greater than or equal to one ($C_F = 1$ when there is no diverging nozzle). The expression for C_F is shown in Eqn. 5.2.

$$C_F = \frac{F_t}{A_t P_c} = \sqrt{\frac{2 k^2}{k-1} \left(\frac{2}{k+1}\right)^{\frac{k+1}{k-1}} \left[1 - \left(\frac{P_e}{P_c}\right)^{\frac{k-1}{k}}\right]} + \left(\frac{P_e - P_a}{P_c}\right) \frac{A_e}{A_t} \quad (5.2)$$

The left term of the equation shows how much the force can be augmented compared to only having the chamber pressure acting over the area of the throat, and can be used to empirically calculate the thrust coefficient. A corollary is that if C_F is known (along with A_t and P_c), it is possible to calculate the thrust generated by a rocket engine. The right term of the equation shows that a theoretical C_F can be computed if the gas properties are known for a given expansion ratio. When the engine operates at optimal expansion, the pressure term on the far right cancels out and the C_F expression yields a maximum value [1].

Since characteristic velocity and the thrust coefficient give the performance of the combustion and the performance of the engine geometry, both can be combined to give the total theoretical engine performance. Using both C^* and C_F , one can calculate the specific impulse by using Eqn. 5.3.

$$I_{sp} = \frac{C^* C_F}{g} \quad (5.3)$$

Consequently, I_{sp} can also be calculated from the thermodynamic properties of the propellants. There are several efficiency factors that affect the performance of both C^* and C_F . For example, combustion losses occur due to irreversibility effects in the combustion chamber (like friction or heat losses) and bad injection quality. Therefore, the C^* efficiency is based on empirical results. Engines of similar design and size have reported C^* efficiency values up to 95% [14]. Additionally, it was previously mentioned that under-expansion or over-expansion reduce performance. This is clear because the C_F relationship yields a maximum when there is optimal expansion. Furthermore, because gases do not exit the divergent nozzle completely axial to the direction of thrust, there is a small loss of thrust. For a conical nozzle with 15° angle, the efficiency of the C_F value is about 98% [5]. To design the chamber and nozzle, it is necessary to take into account these inefficiencies to ensure the engine will match the required performance. Henceforth, the efficiency values used for C^* and C_F are 0.95 and 0.98, respectively.

5.2 DESIGN PROCESS FOR THROTTLING OPERATION

To initiate the design of the chamber and nozzle, it was first necessary to obtain all the gas properties for LOX/LCH₄ combustion. CEA was used to obtain all the combustion product properties and temperatures at different pressures for a specific MR. The output file includes information like combustion temperature, specific heats, and molecular mass. Conveniently, it also performs calculations to output C^* . All these values were recorded and tabulated for pressures between 12.8 – 312.8 psia at a fixed MR of 2.7. Resultant C^* values are around 6000 ft/s for this propellant combination.

The steps taken to determine the rocket engine parameters are described as follows [5]. All equations used are referenced by number in this document.

C1. First the operating pressure is identified for a specific thrust (for example, $P_c = 232.8$ psia at $F = 2000$ lbf thrust). The combustion gas properties are identified at that pressure and inlet conditions (for example, properties used come from CEA at the specified P_c and MR).

C2. Next, the corresponding C_F value is computed using the right side of Eqn. 5.2. This calculation is simplified by first assuming optimal expansion conditions ($P_e = 12.8$ psia). Consequently, the far right pressure term in Eqn. 5.2 cancels out.

C3. The CEA C^* value and the newfound C_F are reduced by their corresponding efficiencies (0.95 & 0.98, respectively). The theoretical I_{sp} is then calculated using Eqn. 5.3.

C4. The theoretical weight flowrate can also be evaluated with Eqn. 3.4 by using the I_{sp} and the corresponding force (in this case 2000 lbf).

C5. Then, the ER can be determined with Eqn. 4.1 at optimal expansion (i.e. $P_e = 12.8$ psia).

C6. Using the C_F , P_c , and F values, one can determine the area of the throat (A_t).

C7. Lastly, the exit area (A_e) is calculated from the ER.

Because the ER, A_e , and A_t values have been defined and remain constant (they are nozzle geometries), it is possible to determine the thrust, I_{sp} , and flowrates at different chamber pressures. The process to do that is shown in the next list.

T1. Using a new P_c and the ER, a new P_e is found by solving for it with Eqn. 4.1. Two solutions are possible for P_e . The correct solution is the pressure smaller than the throat pressure (P_t) dictated by the critical pressure ratio at the new P_c (Eqn. 3.2)

T2. Next a C_F at the new chamber pressure is calculated. Because the exit pressure is different, the pressure term does not cancel out and the new C_F will be lower than the optimal expansion C_F .

T3. Using the new C_F and P_e values along with the fixed A_t value, one can determine the throttled thrust (F) with Eqn. 5.2.

T4. The I_{sp} is computed the same way as step C3 with the C_F and the C^* at the new P_e .

T5. Lastly, the necessary throttled flow rate is computed the same as step C7.

Throttling the engine gives rise to certain issues. As mentioned in previous chapters, the fixed ER value causes different exit pressures. The resultant ER is large when the engine is set to operate at optimum expansion conditions for high end thrust; hence the nozzle is over-expanded. This causes a risky low exit pressure at low end thrust and may cause flow separation, which is undesirable for its potential to cause structural instabilities. According to literature, experiments have shown that flow will normally remain attached to the nozzle if the exit pressure remains $\leq 40\%$ of the ambient pressure [1]. Thus, the goal is to choose an ER that will not lead to an exit pressure less than $0.4P_e$ (5.12 psia in this case). On the other hand, setting optimum expansion at low end thrust results in a low ER. This removes the concern for a low exit pressure because the nozzle will always remain under-expanded. Unfortunately this means that the engine will be operating below optimum performance for the whole thrust range. Based on the C_F equation (Eqn. 5.2), the engine will perform at its lowest at high end thrust due to incomplete gas expansion. Because the high end thrust requires greater P_e , the amount of unconverted pressure into velocity is greater. Moreover, high end thrust requires more propellant flowrate, so low performance at high end thrust results in much more propellant spent than low performance at low thrust. For example, Table 5.1 shows the resultant ER, P_e , and I_{sp} values for optimum expansion at either 2000 lbf or 500 lbf. As stated before, optimum expansion at 2000 lbf leads to a much bigger ER (3.62 vs 1.6), but the exit pressure falls below $0.4P_e$ (5.12 psia). Moreover, optimum expansion at 500 lbf has a high end thrust I_{sp} about 15 seconds smaller than optimum expansion at 2000 lbf. This difference could prove to be a significant propellant expenditure for long duration runs. Certainly, the converse is true: the optimum expansion at 500 lbf has an I_{sp} greater than optimum expansion at 2000 lbf at low end thrust by about 15 seconds. Regardless, low end thrust is four times lower than high end thrust and requires much lower flow rates, so the propellant expenditure at low thrust

is not as significant. Given that optimum expansion at both high and low thrust results in somewhat undesirable results, a compromise between both seemed ideal. Setting the optimum expansion at a thrust level between 2000 – 500 lbf would lead to better compromise between performance and stability.

Table 5.1: ER and I_{sp} for Optimum Expansion for Different Thrusts

Parameter	Optimum Expansion at 500 lbf	Optimum Expansion at 2000 lbf
ER	1.6	3.62
P_c @ 500 lbf	≈ 12.8 psia	≈ 4.5 psia
I_{sp} @ 2000 lbf	≈ 231.4 sec	≈ 246.3
I_{sp} @ 500 lbf	≈ 192.7 sec	≈ 177.7

5.3 MATLAB CODE & PERFORMANCE RESULTS

To determine the ideal optimum expansion thrust level, a MATLAB code was generated that could compute all the mentioned engine parameters at a specified thrust level and a maximum chamber pressure. Employing a code facilitated the calculations for the throttle range of the engine. The code allows the user to input a thrust range (high to low end thrust), a corresponding max chamber pressure, and a desired optimal expansion thrust. The code then iterates to find the ER & A_t that satisfy the input conditions. To find a solution the code first guesses a chamber pressure that would correspond to the optimum expansion thrust input. It then takes the necessary CEA data for a given propellant combination and MR. With those variables it computes all the corresponding engine calculations, and then it compares if the high end thrust would match the specified chamber pressure input (i.e. $P_c = 232.8$ psia at $F = 2000$ lbf thrust). If the results don't match, it employs a numerical false position method and selects a new initial chamber pressure. It iterates until the chamber pressure and thrust inputs are met. The code outputs include the A_t & ER values, and arrays for C^* , C_F , flow rates, expected I_{sp} , chamber pressure, exit pressure, and exit velocities for

the thrust range input specified. Furthermore, the code also includes a FFC percentage input to calculate the overall system I_{sp} of the engine. This is used to ensure that the system I_{sp} requirements are met.

In addition to this, the code has the option to include a contraction ratio (CR) input. The CR is the ratio of the chamber diameter to the throat area. This parameter affects the calculation because in a chamber of definite size the total chamber pressure is reduced before entering the converging-diverging nozzle. This occurs due to effects described by Rayleigh flow. Rayleigh flow is the condition where flow goes through a frictionless constant-area duct but undergoes stagnation temperature change. The temperature change implies heat addition or rejection, differing from an isentropic process. The Rayleigh flow process can be used to model the combustion chamber process because the combustion exothermic reaction can be considered as heat addition to the product gases through a cylindrical (i.e. constant-area) vessel [5]. Based on Rayleigh flow equations, the pressure entering the converging nozzle (or exiting the chamber) is reduced by the following ratio.

$$\frac{P_c}{P_{c,nz}} = \frac{1 + kM_{nz}^2}{\left(1 + \frac{k-1}{2}M_{nz}^2\right)^{\frac{k}{k-1}}} \quad (5.4)$$

In this equation, $P_{c,nz}$ is the nozzle inlet pressure and M_{nz} is the nozzle inlet local Mach number. This equation shows that any Mach number magnitude between zero and 1 would reduce the available chamber pressure before entering the nozzle. This reduction in pressure would reduce the effective exit velocity, and thus performance. Consequently, it is desirable to keep the Mach number low before entering the nozzle. The contraction ratio is used to calculate the Mach number at the nozzle inlet. The relationship between these variables is shown below [5].

$$CR = \frac{A_c}{A_t} = \frac{1}{M_{nz}} \sqrt{\left[\frac{1 + \frac{k-1}{2}M_{nz}^2}{\frac{k+1}{2}} \right]^{\frac{k+1}{k-1}}} ; \quad 0 < M_{nz} \leq 1 \quad (5.5)$$

As a result, specifying a contraction ratio allows the definition of the M_{nz} value, and in turn the chamber pressure loss before entering the nozzle. It is recommended to design engines with

CR values between 3 – 6 to keep the M_{nz} low and reduce losses [1]. For example, the combustion products of LOX/LCH₄ at an MR = 2.7 have a $k \approx 1.14$, and a CR = 4 only produces a theoretical stagnation pressure loss of 1.26%. The MATLAB code computes this loss and reduces the chamber pressure to produce more accurate performance results. If the CR value isn't specified the chamber pressure reduction is neglected.

The code was used to find different engine performance conditions that would match the thrust range and maximum chamber pressure required. Several optimal expansion thrust level inputs were used to determine the best compromise between performance and acceptable exit pressure levels. Other inputs included the C^* & C_F efficiencies, FFC% = 30%, and a CR = 4. After several comparisons, it was deemed that the engine would work best with an optimal expansion thrust of 1250 lbf. Some of the resultant parameters & performance characteristics are shown in Table 5.2.

Table 5.2: Engine Parameters for Optimal Expansion at 1250 lbf Thrust

Parameter	Value
Thrust Range	2000 – 500 lbf
Optimal Expansion Thrust	1250 lbf
P_c	232.8 – 75.2 psia
ER & A_t	ER = 2.7; A_t = 2.85 in
P_e	6.31 psia (49% P_a)
I_{sp}	$\approx 244.4 - 187.6$ s
System I_{sp} (includes 30% FFC)	$\approx 219 - 168$ s
Combustion Flow rates	LOX $\approx 6 - 1.95$ lbf/s LCH ₄ $\approx 2.21 - 0.72$ lbf/s
FFC	FFC LCH ₄ $\approx 0.95 - 0.3$ lbf/s

It is noticeable that the ER is between the values shown in Table 5.1. The flow separation issue is mitigated since the exit pressure well above the $0.4P_a$ limit. Furthermore, I_{sp} values are

within close range of the optimal expansion results at 2000 or 500 lbf. The high thrust I_{sp} is only about 2 seconds lower and the low thrust I_{sp} is only about 5 seconds lower than optimal performance. Lastly, the assumption of 30% FFC kept the system I_{sp} well within the minimum vehicle requirements. Therefore, the choice of optimal expansion at 1250 lbf was deemed acceptable. Figures 5.1 and 5.2 show charts with the expected chamber pressures, total weight flowrates, I_{sp} , and system I_{sp} for the engine.

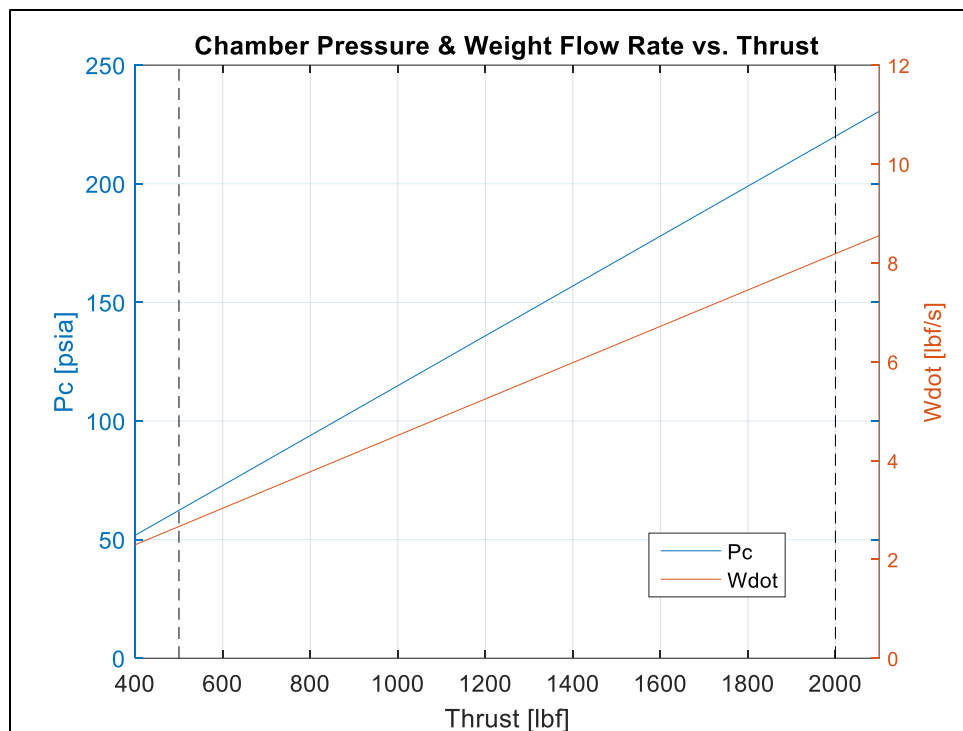


Figure 5.1: Expected Chamber Pressure & Weight Flow rate vs. Thrust

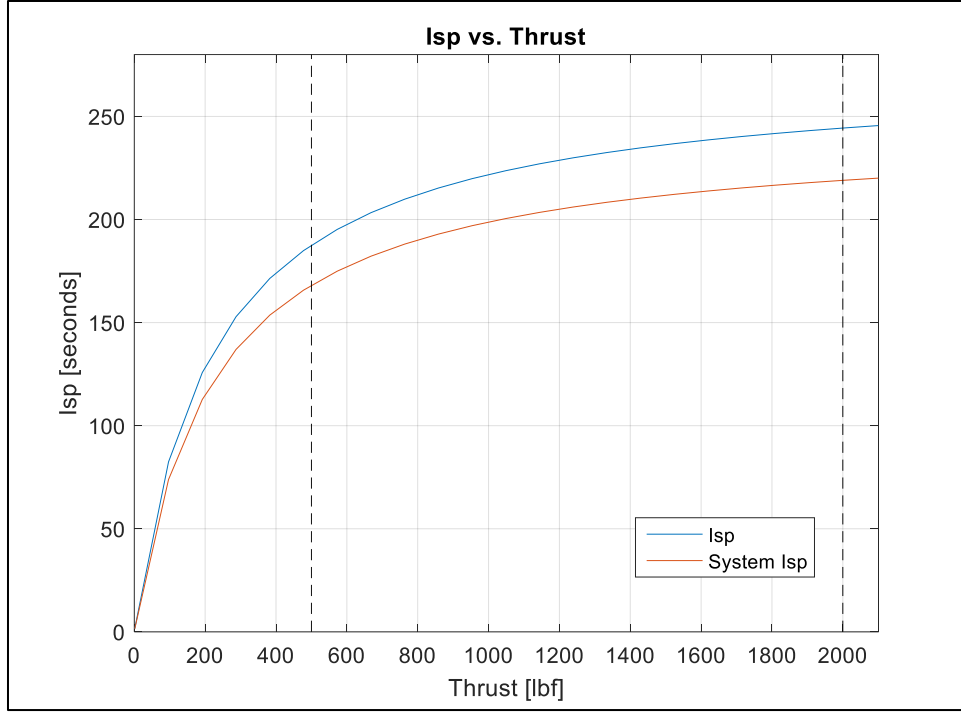


Figure 5.2: Engine I_{sp} vs. Thrust

5.4 COMBUSTOR GEOMETRY DIMENSIONS

Based on the results obtained from the previous section, it became possible to begin design of the chamber and nozzle. Each geometry was defined using mostly empirical design principles from previous engines. The following sections describe these parameters more in detail.

5.4.1 Diverging Nozzle Geometry

The two types of nozzle shape most widely used are conical and bell nozzles. Conical nozzles have a diverging section that expand linearly (hence conical). A typical conical nozzle configuration is shown in Figure 5.3. Most conical nozzles have a circular arc on top of the throat that is about 0.5 to 1.5 times the throat radius (R_t). The nozzle then extends at an angle, usually between 12 to 18°, but 15 is usually the standard for comparison. Because the gas does not exit the nozzle completely axially, there is a divergence loss and the efficiency drops. The thrust efficiency is expressed as shown in Eqn. 5.6 [5]. In that equation λ is the thrust efficiency and α is the

divergence angle. For 15° conical nozzles this results in a nozzle thrust efficiency of $\lambda = 0.983$. Hence the C_F efficiency of 98% for optimal expansion [5].

$$\lambda = 0.5(1 + \cos \alpha) \quad (5.6)$$

A bell nozzle configuration is shown in Figure 5.4. A more common contemporary configuration, these nozzles were created to produce better performance than a conical one. The big divergence angle right after the throat minimize energy losses from the quick expanding gases, and then the contour inflects to a lower angle to decrease the divergence loss as the gas exits. The divergence angles (θ_n and θ_e) are determined from a process called the method of characteristics, which assesses how to minimize energy losses from the expansion waves inside the nozzle. These values are usually reported for a given ER and nozzle length [1]. Because of its parabolic shape, the bell nozzle is generally smaller than the conical nozzle. The bell nozzle length is usually reported as a percentage of the total length of a cone nozzle with equivalent ER, A_e , and A_t . This is usually 80% of the equivalent 15° cone nozzle. The bell nozzle thrust efficiency is similar to the conical equivalent; for example, an 80% bell nozzle has a $\lambda = 0.985$. A smaller nozzle implies less weight, making the bell nozzle more attractive for big ER values. The main drawback is that the contoured shape proves more difficult to manufacture [1].

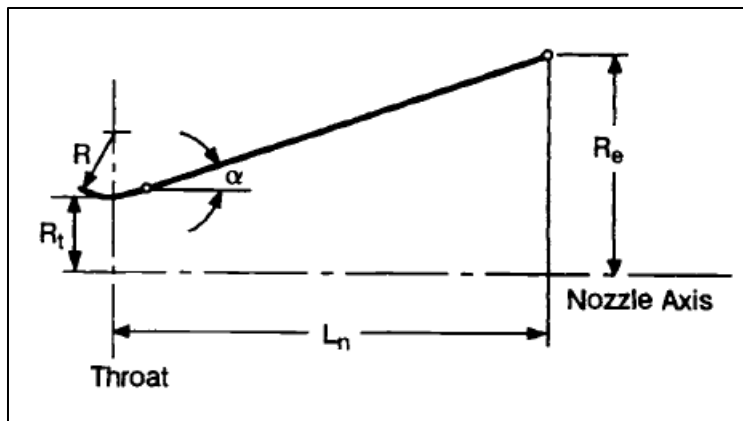


Figure 5.3: Conical Nozzle Shape [5]

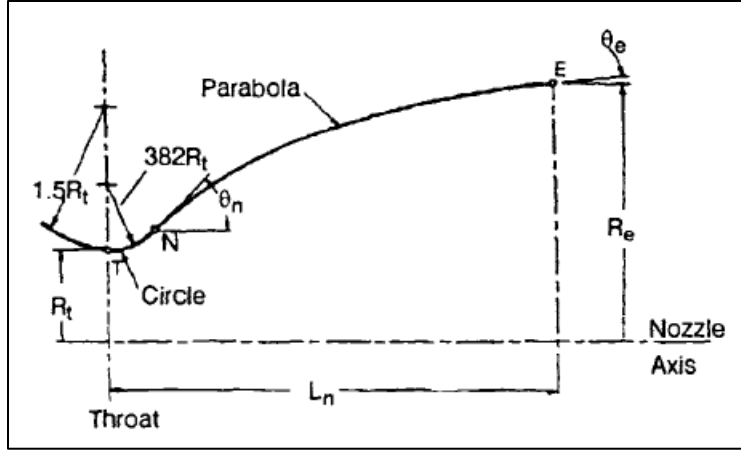


Figure 5.4: Bell Nozzle Contour [5]

To compare the two nozzle types for this application, the length and shape of a conical 15° nozzle with the engine ER and exit/throat dimensions were calculated and drawn. Then, an 80% bell nozzle was designed using the corresponding equivalent parameters. The equivalent divergence angle for a bell nozzle were obtained using tables found literature [1]. The resulting geometries are described in Table 5.3 and the contours are shown in Figure 5.5.

Table 5.3: Cone Nozzle vs Bell Nozzle Geometries

Parameter	15° Cone Nozzle	80% Bell Nozzle
Length	3.52 in	2.80 in
Circular Arc Radius	0.713 in ($0.5R_t$)	0.544 in ($0.382R_t$)
Divergence Angle	$\alpha = 15$	$\theta_n = 22.5^\circ$ $\theta_e = 17.7^\circ$

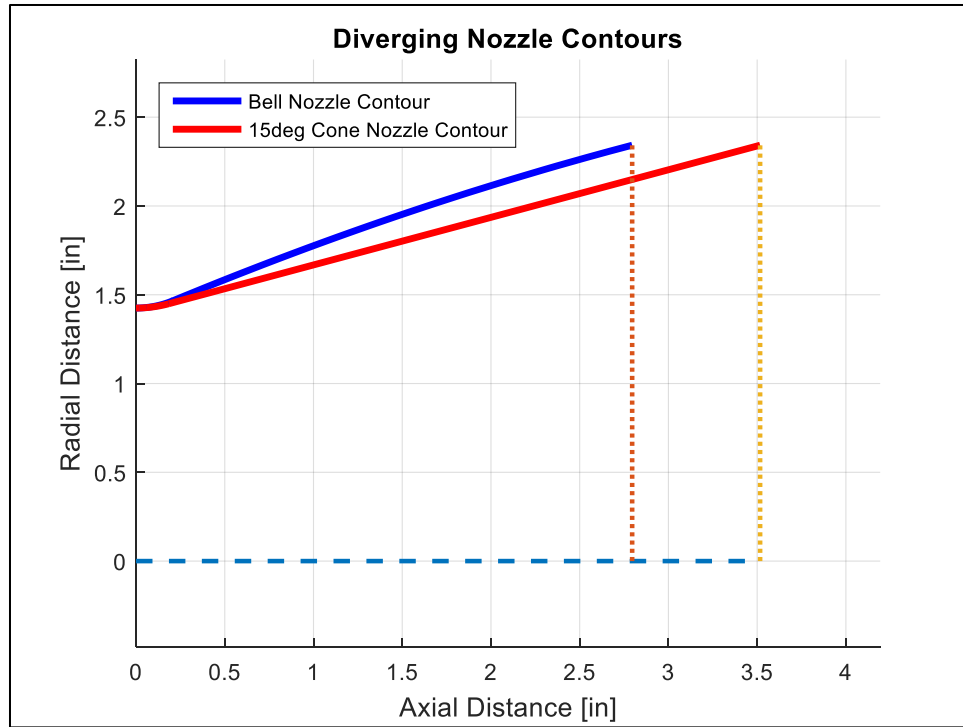


Figure 5.5: Comparison of Cone Nozzle vs Bell Nozzle for CROME-X

As seen in Figure 5.5 the contour of both diverging nozzle shapes look almost equivalent at such a small expansion ratio. Additionally, the length difference is less than one inch. Therefore, the conical nozzle was chosen, due to its relative simplicity and ease of manufacturing.

5.4.2 Chamber & Converging Nozzle Design

Conventionally, most rocket engines have a cylindrical combustion chamber. Spherical and near spherical combustion chambers have been used before. They provide less cooling requirements and experience less mechanical stress due to smaller a surface area and better stress distribution. Nevertheless, it is much more difficult to manufacture a spherical chamber and some engines have shown poorer performance compared to the cylindrical shape [5]. Consequently, a cylindrical chamber will be used for this engine.

The chamber diameter was easily defined using the CR value specified in the performance calculations conducted before. Using the $CR = 4$ and the $A_t = 2.85$ in, the chamber diameter should be 5.7 inches. The convergence angle for most engines vary from 20 to 45°. To provide a smoother

nozzle flow an angle of 35° was chosen. The convergence arc radius at the throat was specified from the conical divergent nozzle parameters of $1.5R_t$. The arc radius at the entrance of the nozzle was kept the same for simplicity.

The chamber cylinder (or barrel) length was defined using an empirical parameter called characteristic length (L^*). L^* is an indication of the propellant residence time in the combustion chamber. It is called characteristic length because it has units of length, and it is defined by the following expression.

$$L^* = \frac{V_c}{A_t} = \frac{\dot{m}t_s}{\rho A_t} \quad (5.7)$$

In this equation V_c is the chamber volume (including the converging section of the nozzle), t_s is the residence time of the propellant, and ρ is the combustion gas density. Residence time is significant to chamber design because it dictates how long the propellants should be in the chamber to fully combust. A small chamber leads to a short residence time (small L^*) and incomplete combustion and lower performance. A long chamber grants longer residence time (large L^*) and might allow full combustion, but it becomes heavier and a bigger size requires more cooling (i.e. performance losses) [1]. L^* is predominantly an empirical value and is based on experience with similar propellants and engine size. From a tests conducted at NASA JSC with an engine of similar size and propellant type, it was revealed that an L^* of 20 – 30 inches would suffice [13]. Consequently, a barrel length of 6 inches was chosen. This length and converging nozzle result in an L^* of ≈ 32 in. This length was deemed acceptable for the first version of the engine.

To determine the thickness of the chamber, thin-wall pressure vessel assumptions were made. This relies upon the assumption that the internal diameter to thickness ratio is ≤ 10 . Moreover, a constant thickness was assumed to occur throughout the length of the whole chamber and nozzle. An initial thickness of 0.2” was used along with the maximum operating P_c and the radius of the chamber. From these quantities, the longitudinal and hoop stress acting on the cylindrical wall were employed to compute an equivalent von Mises stress. This equivalent stress is computed as shown in Eqn. 5.8 [18].

$$\sigma_{vm} = \frac{\sqrt{3} P_c R_c}{2 t h_c} \quad (5.8)$$

In this equation, R_c is the radius of the chamber and $t h_c$ is the chamber thickness. When the resultant von Mises stress is compared against the yield strength of Inconel 718 (≈ 11.5 ksi @ 2000 °F), the factor of safety is around 3.4. Because the ratio of thickness to the chamber radius is 14.25, the thin pressure vessel assumption is valid. Further analysis and FEA will be conducted to assess stress concentrations, pressure spikes, and the effect of thermal stress caused by thermal gradients in the chamber. A drawing of the engine chamber and nozzle is shown in Figure 5.6 and a picture in Figure 5.7.

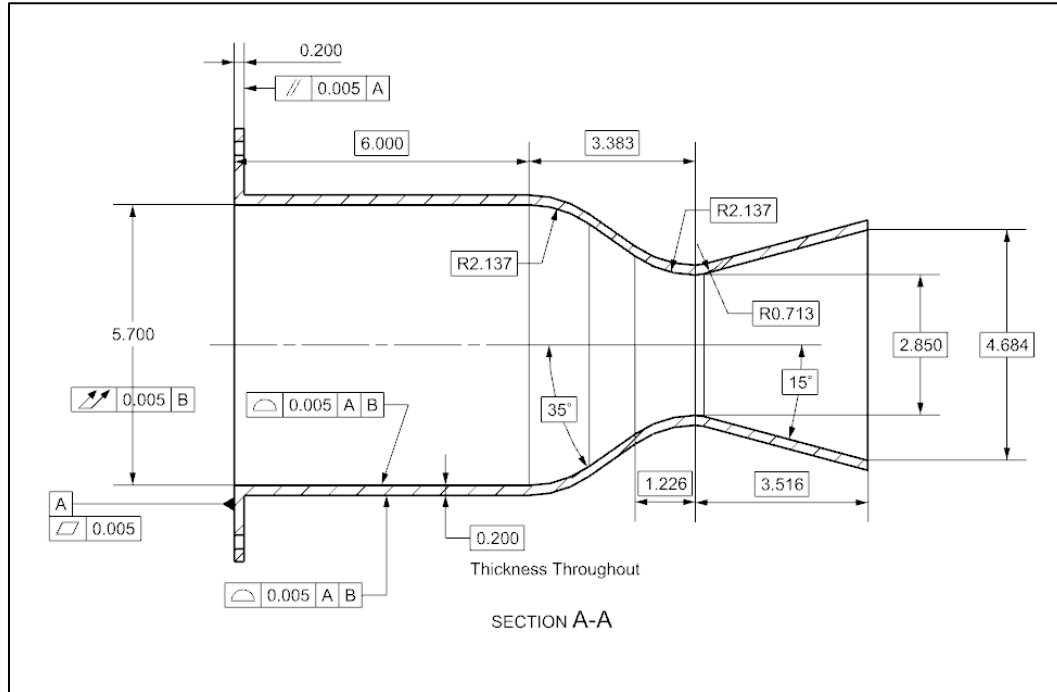


Figure 5.6: Dimensions of the Combustion Chamber and Nozzle

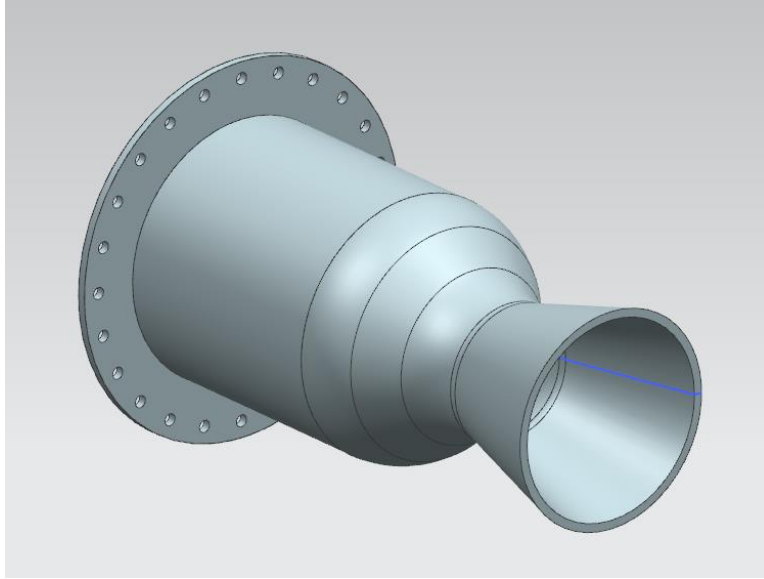


Figure 5.7: Chamber and Nozzle for CROME-X

Chapter 6: Injector Selection and Design

The following chapter discusses the design of the injector used for CROME-X. The next sections will first describe the role of the injector and its mechanism for operation. Next, different types of injector will be compared and the selection criteria used to select one. Ultimately, a pintle type injector was chosen. Subsequently, the design criteria and process is explained. This includes design of the injection orifices, FFC orifices, and acoustic cavities.

6.1 INJECTION PURPOSE, TYPES, AND SELECTION CRITERIA

The injector is the component that introduces the propellants into the combustion chamber. Specifically, it injects the oxidizer, fuel, and coolant at the correct proportions and the necessary conditions (e.g. velocity, angle, temperature, pressure, etc.) to promote stable & efficient combustion [4]. Most liquid propellants do not readily combust in liquid form. Injecting the propellants at high velocity promotes atomization (the process of breaking up the propellant into small droplets), enabling combustion. Consequently, the injector has the greatest impact on combustion efficiency (C^*) and engine performance [1]. Furthermore, combustion stability is highly dependent on the injection element type and injection flow resistance (i.e. injection pressure drop) [5]. To prevent destructive instabilities, it is critical to select the correct injector for a specific application and design the injection parameters accordingly.

There are different injector types used in practice. Some of these are shown in Figure 6.1. Showerhead type injectors have elements that deliver the propellants through small orifices axially from the injector face into the combustion chamber. This type provides poor atomization and is not commonly used. Impinging type injectors prevent this issue by angling the injection holes and impinging the propellant jets. This method enables good mixing and combustion performance, but the injection geometries are generally difficult to manufacture and sensitive to machining tolerances. Impinging injector configurations include the self-impinging, doublet, and triplet impinging. Coaxial injector types employ several elements that flow a liquid propellant and a gas propellant. The liquid propellant flows through a central port and the gaseous propellant flows

through an annular element. The gas flows at speeds much faster than the liquid; upon injection the speed difference causes a shear action that helps break down the liquid. This injection method also provides good combustion efficiency, but it is limited to liquid/gas propellant configurations and annular geometries can be difficult to fabricate [5] [1].

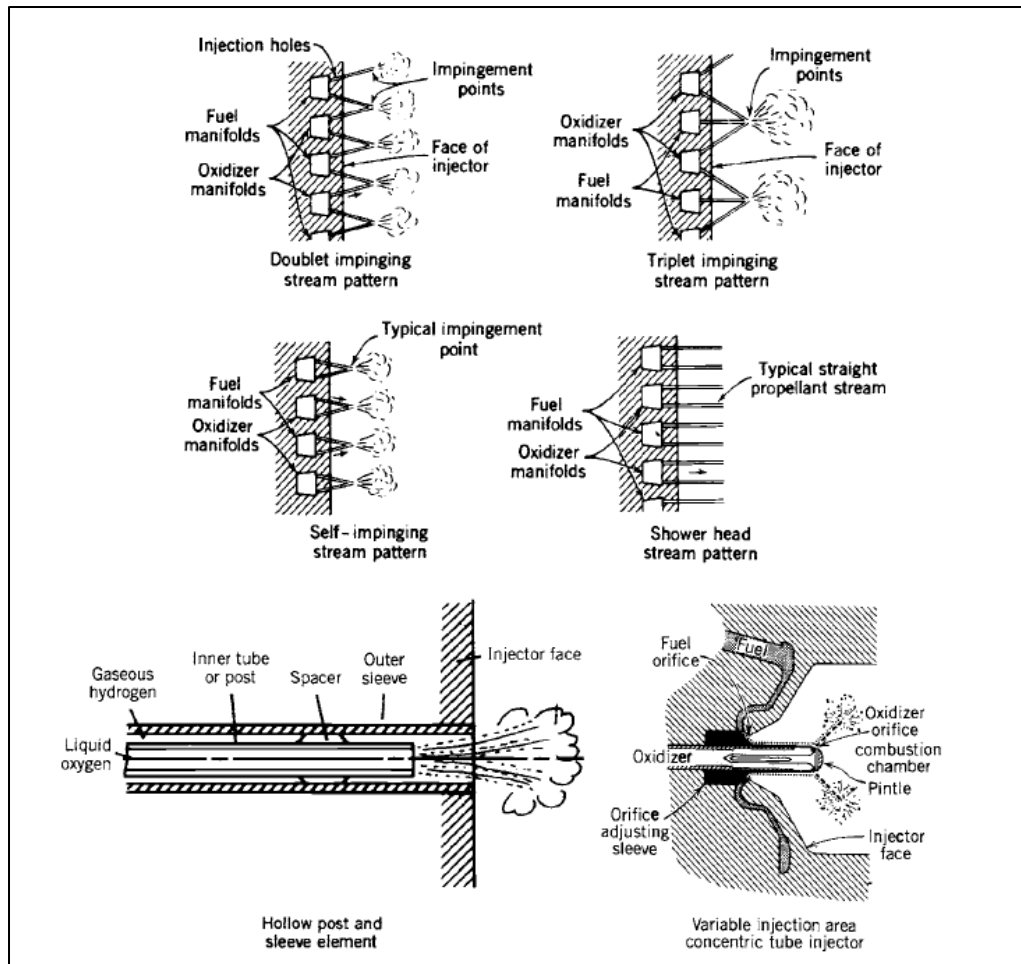


Figure 6.1: Different Injector Configurations [1]

After careful deliberation, a pintle type injector was selected for CROME-X. This type of injector has two injection elements: an annular and a radial port. The radial flow travels axially through a central port and is then distributed radially by redirecting the flow through an internal contoured surface at the pintle tip. The annular flow travels through an annular orifice surrounding

the central channel. Both the radial and annular flow impinge and form a conical spray into the combustion chamber. This injection process is illustrated in Figure 6.2.

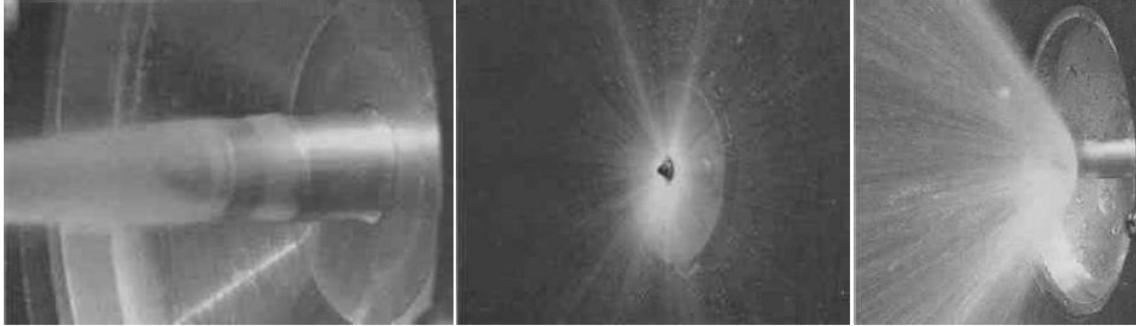


Figure 6.2: Injection Spray of a Pintle Injector (Annular, Radial, and Combined Flow) [19]

Historically, the pintle injector has demonstrated several advantages. First, pintle injectors have deep throttling capabilities. Previous pintle designs have demonstrated stable throttle ratios of 40:1 or larger. Second, pintle type injectors are inherently stable. Unlike other injector types, there has been very few occurrences of engine failures caused by a pintle injector instability. Third, pintle injectors are generally less expensive to fabricate when compared to impinging or coaxial types because they have a simpler design. Although pintles are not as efficient as other injector types, the pintle injector was chosen for the first version of the engine given its stability, cost, and throttling advantages [19] [5]. It is noteworthy to mention that only the first version of CROME-X will use a pintle injector. A coaxial injector will be used for future engine models that use regenerative cooling. Regenerative cooling will likely gasify the propellant fuel as it cools the engine, and the liquid/gas configuration is more adequate for a coaxial type injection element.

Most pintle injectors use movable sleeves and components to change the injection area and throttle the engine. As previously stated, the engine will use the main valves for throttling. Consequently, the CROME-X pintle design will have a fixed geometry and injection area. The following sections describe the injector design process.

6.2 PINTLE INJECTION DESIGN

The following section discusses general criteria for injector design. This focuses mostly on injection area and injector pressure drop. The subsequent section discusses design criteria pertinent to pintle injectors. Lastly it shows some of the geometries derived from the mentioned criteria.

6.2.1 General Injector Design criteria

In an injector with fixed geometry, the flow characteristics are controlled by the injection area. At a given flow rate, the area of injection will define the injection velocity and pressure for a specific fluid [20]. Conversely, if a specific pressure drop or velocity is required, one can calculate the necessary area of injection. Eqn. 6.1 shows the relationship between these quantities for an injection element of a specific propellant (oxidizer or fuel) [5].

$$A_{inj} = \dot{w} \sqrt{\frac{2.238K}{\rho \Delta P}} \quad (6.1)$$

Here A_{inj} is the total area of injection (in^2), \dot{w} is either the oxidizer or fuel weight flow rate (lbf/s), K is the minor loss coefficient across the injection element, ρ is the density of the oxidizer or fuel (lbm/ft^3), and ΔP is the pressure loss across the injector orifice (psi). This equation is derived from the Bernoulli equation, and it applies when the upstream velocity is much lower than the injection orifice velocity. The total area of injection applies to all the geometries that inject the propellant. Thus, the sum of all the injection elements should equal A_{inj} . The K value takes into account any losses caused by disruptions or changes to the flow (e.g. reentrant, contraction, & exit losses), and values are commonly found for different geometries [20]. Moreover, even though FFC is not essentially an injection combustion element, FFC injection ports follow the same principles. Therefore, the FFC injection area is computed the same way as the combustion injection elements [5]. Once an injection area is computed, the flow velocity can be found from mass conservation (Eqn. 6.2).

$$\dot{m} = \rho v_{inj} A_{inj} \quad (6.2)$$

In this equation \dot{m} is the mass flow rate of the oxidizer or fuel, and v_{inj} is the propellant injection velocity. Once the flow rates of the propellants and the injection exit conditions (i.e. density) are defined, the injection area and velocity can be determined for a given pressure drop.

Special mention should be made about injection flow resistance (or pressure drop). Based on experiments and observations, a certain level of pressure drop is needed to prevent the onset of low-frequency instabilities (also called chug). Chug is the effect caused when a pressure disturbance in the combustion chamber disrupts the upstream pressure, thus disrupting the propellant flow. This can cause flow oscillations that affect the engine performance. As a rule of thumb, the injector pressure drop is normally designed to be about 20% chamber pressure (dP/P_c). This ensures that most chamber pressure spikes and/or oscillations remain below the inlet pressure of the injector orifices, and the flow is uninterrupted [5]. Unfortunately, the dP/P_c value can't be too large either because it could trigger the onset of high-frequency combustion instabilities. High-frequency instabilities are destructive in nature and pose a real danger to engine integrity [5]. This type of instabilities will be discussed more in detail in later sections.

Throttling poses an issue with maintaining an ideal dP/P_c value. It was mentioned in previous chapters that P_c changes approximately proportional with flow. It is evident from Eqn. 6.1 that as the flow rate changes, the injector ΔP changes as the square of the flow [5]. When the engine is throttled down, dP/P_c drops as well. Thus, low throttle levels have the tendency to trigger chug. Moreover, designing the orifices for a high dP/P_c at low thrust could lead to a dangerously big dP/P_c value at high end thrust. To ensure stability throughout, there is the need to select an injection area that satisfies both low and high thrust conditions. Results obtained from several LOX/LCH₄ engines of similar design and size at JSC demonstrated that a dP/P_c between 9 – 32% proved stable [14]. Therefore, a similar pressure drop range will be used for CROME-X.

Several areas were calculated based on the weight flow rate vs. thrust correlations developed (shown in the previous chapter). For each area, the dP/P_c curve vs. flow rate (i.e. thrust) was created to evaluate if the pressure drop percentage was somewhat near the 9 – 32% range. The propellant densities used were obtained from REFPROP at the expected chamber pressure and

saturation temperature for a given flow rate. To total minor loss coefficient used was $K = 1.7$ (0.5 entrance loss, 0.2 running friction loss, and 1.0 exit loss for an injection orifice) [5]. Moreover, the ΔP was kept the same for the LOX, the LCH₄, and the FFC to ensure even flow through the manifolds.

After several iterations, it was determined that the ideal injection areas would be set to operate at 20% dP/P_c during optimal expansion thrust ($F_{opt} = 1250$ lbf). This resulted in a dP/P_c between 9.9 – 30% from low to high end thrust. The propellant properties, resultant areas of injection, and thrust range dP/P_c limits are shown in Table 6.1. Figure 6.3 also shows the dP/P_c distribution for the operating thrust range. Since the areas have been defined, the next section shows how other pintle injection geometries were defined.

Table 6.1: Propellant Properties & Injection Parameters

Parameter	Value
Density @ $F_{opt} = 1250$ lbf	LOX: 71.37 lbs/ft ³ LCH ₄ : 26.43 lbs/ft ³
Injection Areas	LOX: 0.165 in ² LCH ₄ : 0.100 in ² FFC: 0.043 in ³
Injection Velocity (v_{inj})	LOX: 71.0 – 23.8 ft/s LCH ₄ : 120 – 39.2 ft/s FFC: 120 – 39.2 ft/s
ΔP (2000 – 500 lbf)	69.9 – 7.4 psi
dP/P_c (2000 – 500 lbf)	30.0 – 9.9 %

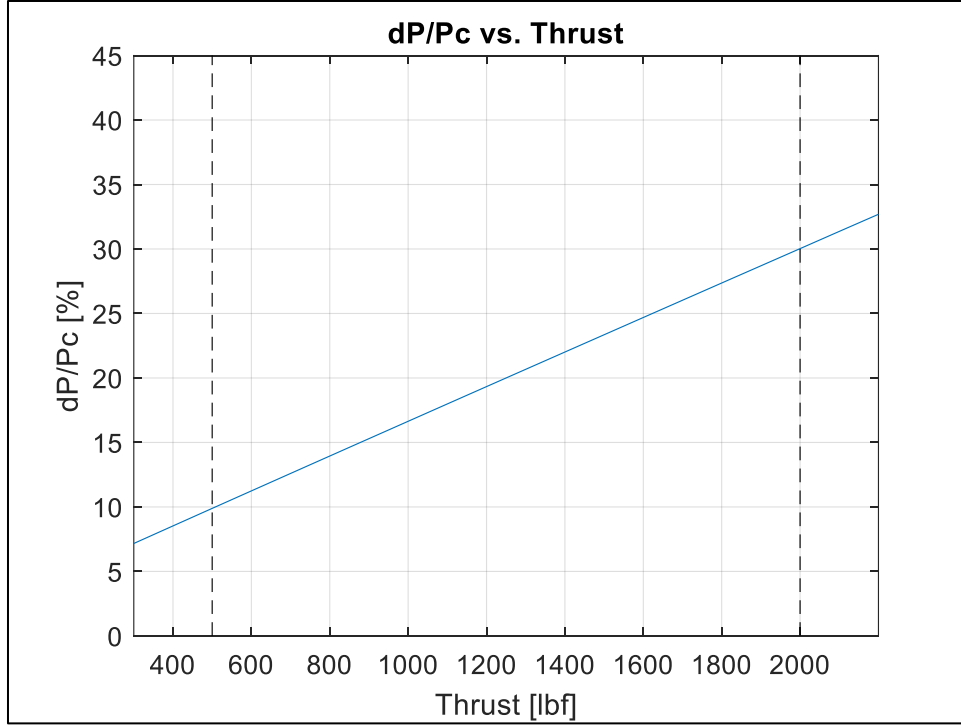


Figure 6.3: dP/P_c vs Thrust for the Injection Areas

6.2.2 Pintle Geometry Design

As mentioned before, pintle injectors collide two propellant jet streams to form a conical spray angle. The spray angle is based on the total momentum ration (TMR). The relationship for TMR is shown in Eqn. 6.3 [21].

$$TMR = \frac{(\dot{m}v_{inj})_{radial}}{(\dot{m}v_{inj})_{annular}} \quad (6.3)$$

Thus, the TMR is the ratio of the radial flow to the annular flow coming from the injector. The jet momentum is just the product of the mass flow rate and the injection velocity. As a result, the angle of the conical spray depends on the TMR (Figure 6.4). A larger TMR produces a wider angle, whereas a smaller TMR a shallower angle. According to literature, a $TMR = 1$ produces optimal injector performance. To estimate the spray angle from the TMR, it is assumed that the angle produced is just the summation of the momentum vectors. This results in the Eqn. 6.4.

$$\theta = \tan^{-1}(TMR) \quad (6.4)$$

Designating either the LOX or the LCH₄ as the radial or the annular flow allows comparison of the TMR and the expected resultant angle. The resulting TMR is calculated using the velocities and flow rates computed before. If the LOX is used as the radial propellant (called a LOX-centered configuration), the TMR = 1.64 and the estimate angle $\theta \approx 58.7^\circ$. In contrast, if the LCH₄ is used as the radial propellant (LCH₄-centered), the TMR = 0.61 and the estimate angle $\theta \approx 31.3^\circ$. A LOX-centered design produces a wider angle and will likely cause the propellant to impinge the chamber wall closer to the injector than a LCH₄-centered design would. Impingement of the propellant closer to the injector is undesirable because it disrupts FFC and can cause damage due to localized combustion [21]. Furthermore, the LCH₄ injection area is smaller than the LOX area. Using the propellant with smaller area for the annular flow is more sensitive to tolerances and tends to increase the velocity and ΔP uncertainties considerably [22]. For these reasons, the design was set to be LCH₄-centered.

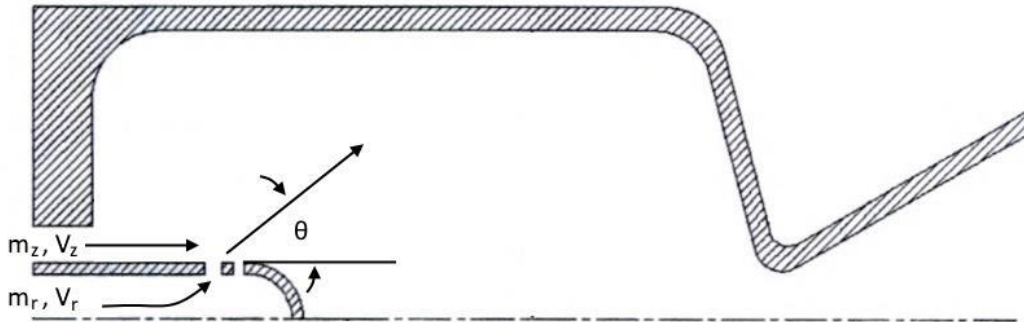


Figure 6.4: Pintle Injection Jets and Spray Angle [21]

Other important parameters are the skip distance ratio (SDR) and the chamber-to-pintle ratio (CPR) of the pintle post. The SDR is the ratio of the length the annular flow has to travel before impacting the radial flow (denoted as skip distance, or L_s) to the diameter of the pintle post (d_p). From empirical studies it was deemed that the optimal SDR = 1. Larger skip distances are undesirable because the annular flow will decelerate due to friction and will result in a wider spray angle. The CPR is the ratio of the chamber diameter (D_c) to the pintle post diameter (d_p). In practice

values for the CPR range from 3 to 5. These equations are shown below, and dimensions for this values are shown in Figure 6.5 [21].

$$SDR = \frac{L_s}{d_p} \quad \& \quad CPR = \frac{D_c}{d_p} \quad (6.5)$$

After assessing different sizes, it was determined that the pintle post diameter would be set to be 0.75 inches. The skip distance was therefore set at 0.75 inches to maintain a SDR value of unity. From the chamber diameter ($D_c = 5.7$ in), it was determined that the $CPR = 7.6$. This number is unconventionally large, but it was deemed acceptable because the annular orifice width (the difference between the major and minor radii of the annulus; denoted as t_{an}) would be too small if the pintle post was any bigger. From geometry, using the LOX area of injection and the minor diameter (d_p) at 0.75 inches yields a $t_{an} = 0.064$ inches.

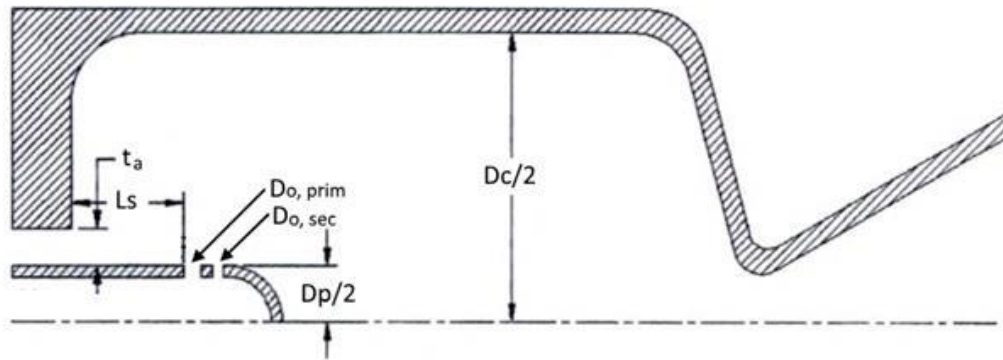


Figure 6.5: Pintle Injector Dimensions [21]

The blockage factor (BF) was used to determine the radial orifice size. The BF is the ratio of the total radial hole diametric length to the circumference of the pintle post [21]. This is shown in Eqn. 6.6. Typically pintles have around 20 – 36 holes, and from experience BF values range from 0.3 to 0.7 [23]. Furthermore, some designs employ two rows of holes. Primary holes (first row) are generally larger, while secondary holes (second row) are smaller and fit within the primary hole gaps [23]. This configuration is seen in Figure 6.6.

$$BF = \frac{N d_o}{\pi d_p} \quad (6.6)$$

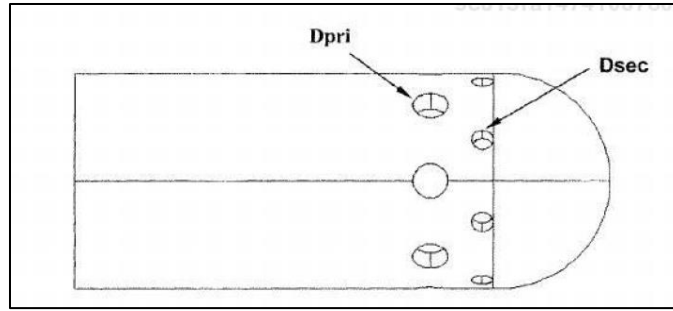


Figure 6.6: Pintle Primary and Secondary Radial Holes [21]

Based on these parameters a set of radial injection holes was designed. Also, the primary/secondary holes approach was used. A total of 24 holes were sized using the LCH_4 area of injection. After comparing different sizes, the orifice dimensions selected are 0.086 inches and 0.057 inches for the primary and secondary holes, respectively. This yields a $\text{BF} = 0.73$, which is close to the conventional range employed.

The orifice alignment was set to be staggered to improve with stress distribution and manufacturing. FEA analysis will be conducted later to address the appropriate thickness for the pintle post. Moreover, the internal contour of the pintle tip is tentative and will require testing to ensure acceptable radial flow distribution. Figure 6.7 shows a picture of the current pintle post configuration.



Figure 6.7: CROME-X Pintle Post Radial Orifices

Next, the annular orifice length was defined. This length needs to be long enough to prevent a condition called hydraulic flip. Hydraulic flip is the phenomenon where there is detachment of the propellant jet from the orifice wall. This leads to a sudden drop of the discharge coefficient, high injection velocities and unstable flow conditions. Based on previous experiments, hydraulic flip should be mitigated if the orifice length is ≥ 4 times the hydraulic diameter of the orifice [24] [14]. For an annular orifice, the hydraulic diameter is equal to the orifice width (t_{an}). Thus, the annular length was set to be 0.26 inches (4 times the value of t_{an}).

Film cooling is essential to keep the integrity of the engine. Thus, the cooling ports are just as significant as the injection orifice holes. Adequate distribution is necessary to ensure all of the chamber circumference is covered by the cooling film. The engine will have a total of 30 film cooling orifices, resulting in a FFC orifice diameter of 0.042 inches. This number was based on manufacturing constraints, and if necessary, more holes can be added to the injector. Moreover, the injection angle of the ports was set equal to 15° outward axial chamber direction to impinge the wall about 0.34 inches below the injection point.

6.3 INJECTOR ASSEMBLY & TESTING FEATURES

An assembly of the injector with all injection features is shown below. All injection geometries and their location is shown as well. As mentioned before, the injector will be made out of Inconel 625. It can be seen that the injector is mostly composed of a series of plates. These plates will fit into each other to come together as one. With the exception of the pintle post, all components will be welded to prevent inter-propellant leaks. The bottom injector body will include the FFC orifices and the annular port. Moreover, the headend of the injector is curved. The face is slightly round to promote propellant recirculation zones, which keep the injector face cooler [23]. The sides will house dog-leg acoustic cavity blocks to prevent instability onsets. The top of the injector will be sealed with a plate that houses the pintle port, igniter port, and the LOX and FFC inlet.

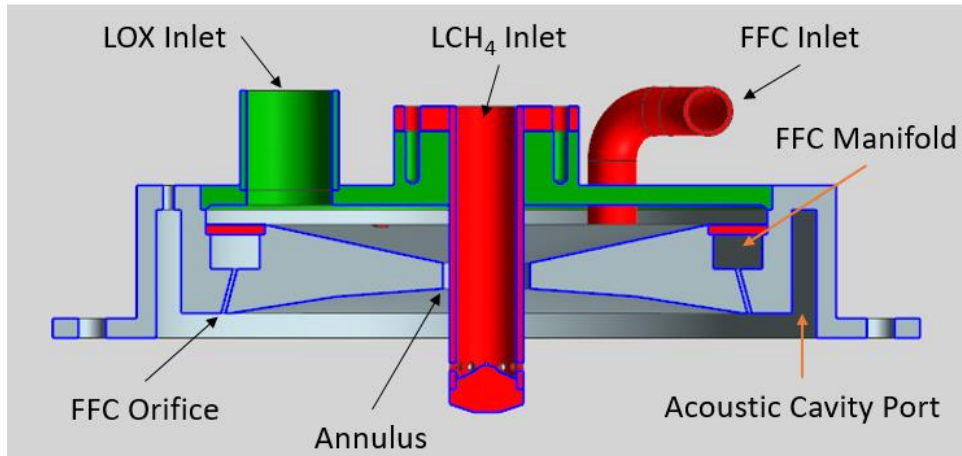


Figure 6.8: Pintle Injector Cross Section View

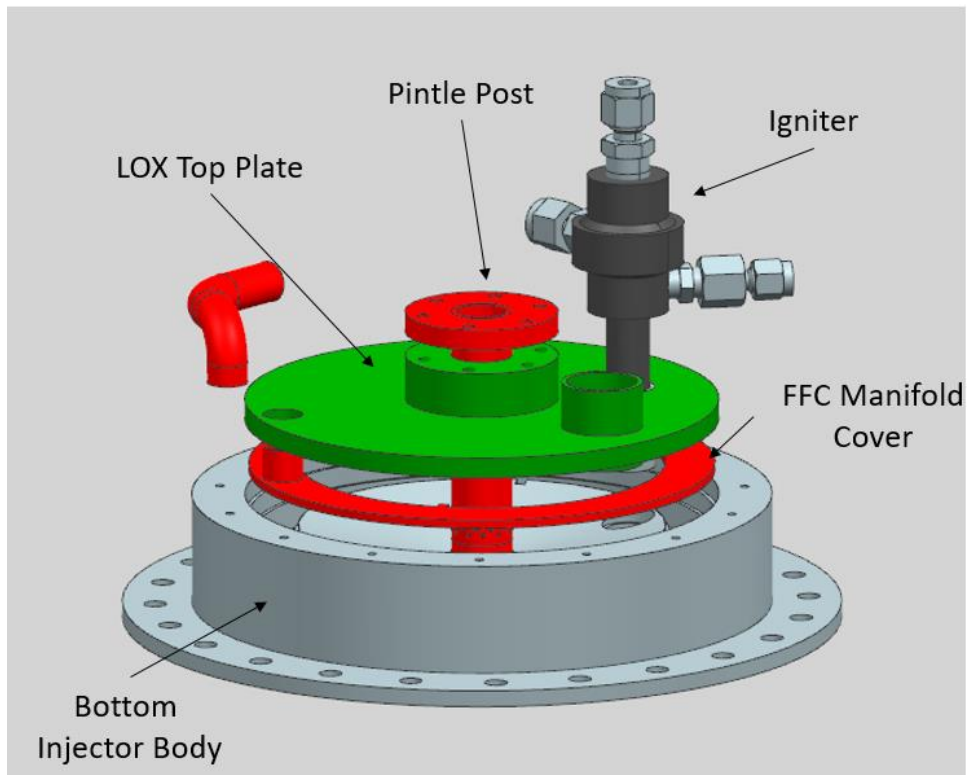


Figure 6.9: Pintle Injector Assembly Exploded View

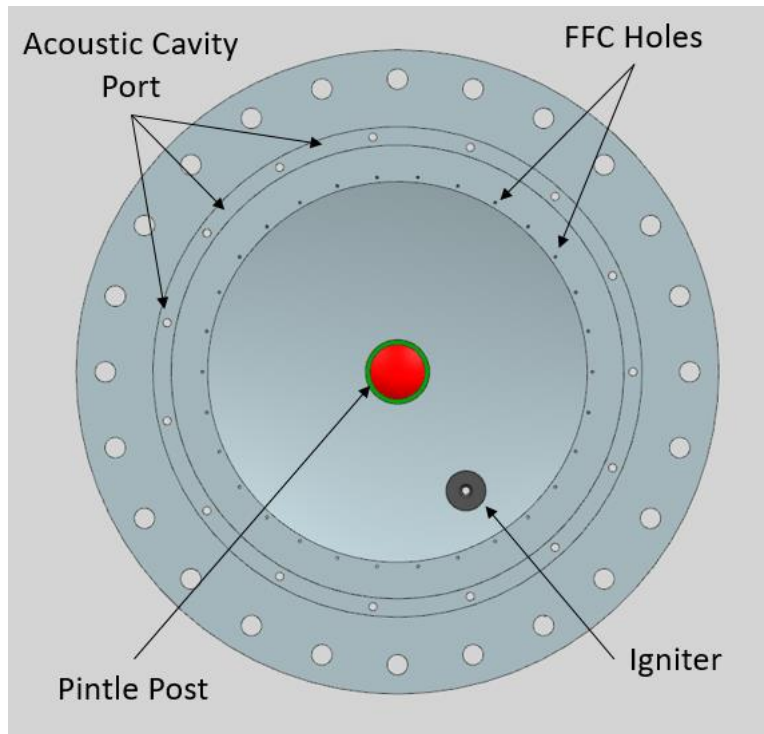


Figure 6.10: Pintle Injector Bottom View

The LOX will be introduced from a 1" OD tube inlet into a dome-like cavity that will direct the flow towards the central annulus. The LCH₄ will be fed directly into the pintle post from a 3/4" OD tube inlet above it. The bottom injector body will house the FFC manifold internally to allow the fluid components (e.g. valves & fittings) to sit on top of the injector. A 1/2" OD tube will bypass the LOX cavity manifold and be fed directly into the FFC manifold. The FFC inlet is therefore on top of the engine and separate from the LCH₄ combustion manifold. The combustion LCH₄ and FFC flows have independent inlets to allow adjustment of the cooling flow rate as necessary.

A LOX/LCH₄ swirl torch igniter developed at cSETR will be used to ignite the propellants. The igniter will sit on top of the injector and relatively close to the pintle post. This was done to ignite the flame as close as possible from the injector head end in the hopes of preventing localized combustion at the wall and promote quick ignition of the engine [21]. The igniter snout will be inserted through the injector top and be welded at both the bottom and top of the injector body. The igniter propellant inlets and sparker will be facing outward towards its delivery lines.

The pintle will be introduced into the top plate of the injector. The top plate will have a cylindrical bore with a transitional fit used to center the pintle post and ensure that the annulus and pintle are aligned. The pintle-injector interface will use a flanged connection. The pintle will be sandwiched between the injector top and the LCH₄ manifold and fastened with 6 x #8-32 screws. All surfaces will be sealed using a PTFE joint sealant called GORE seal. This sealing material is ideal for flange connections and works well with cryogenic propellants [25]. The GORE seal will also be employed for the injector-chamber flange, and tests will be conducted to ensure that it seals properly at high temperature applications.

6.3.1 Testing features

Because this is the first version of CROME-X, several features are focused on modularity and testing to ensure safe operation and improve performance. These aspects will be studied and improved for future versions of the engine. Specifically, the injector has the capability to exchange the pintle and the acoustic cavity blocks. This is discussed more in detail in the following section.

6.3.1.1 Pintle Modularity

The injector has the capability to remove and exchange the pintle. This design decision was made to allow testing of different injector geometries. The specific geometry features that can be tested with different pintle posts are listed below.

- Different injection orifice geometry. The injection geometry has a direct effect on combustion performance (i.e. propellant atomization). Different orifice size, shape, and configuration can be adjusted.
- The effect of different skip distances. Pintles with different length can be tested to evaluate the length effect on spray characteristics like jet breakup and spray angle.
- Annulus of different diameters. Although the annulus geometry is fixed, the pintle diameter can be varied to adjust the annulus injection area. This can be used to assess different pressure drops or MRs.

Pintle tip failure is also a concern for pintle injectors. Failure can occur due to concentrated heat flux on the tip caused by recirculation of the combustion gases [21]. Thus, if any failure occurs the pintle post can be replaced. Furthermore, implementing additive manufacturing is of interest for this project. Hence, 3D printed pintle posts can be fabricated and tested as well.

6.3.1.2 Acoustic cavity blocks

Combustion instabilities are caused by pressure fluctuations in the combustion chamber and reduce the efficiency in which propellant energy is converted to thrust [8]. If the pressure fluctuations resonate with the engine acoustics then excessive vibration forces or heat transfer might occur and trigger engine failure [1]. There are three types of instability that pertain to rocket engines: low, medium, and high-frequency combustion instabilities. Low and medium frequency instabilities can affect performance, but are not generally destructive. On the other hand, high-frequency instabilities are highly destructive. A description of each instability is shown in Figure 6.11.

Type and Word Description	Frequency Range (Hz)	Cause Relationship
Low frequency, called chugging or feed system instability	10–400	Linked with pressure interactions between propellant feed system, if not the entire vehicle, and combustion chamber
Intermediate frequency, called acoustic, ^a buzzing, or entropy waves	400–1000	Linked with mechanical vibrations of propulsion structure, injector manifold, flow eddies, fuel/oxidizer ratio fluctuations, and propellant feed system resonances
High frequency, called screaming, screeching, or squealing	Above 1000	Linked with combustion process forces (pressure waves) and chamber acoustical resonance properties

^aUse of the word *acoustical* stems from the fact the frequency of the oscillations is related to combustion chamber dimensions and velocity of sound in the combustion gas.

Figure 6.11: Combustion Instability Types and Description [1]

Acoustic cavities are devices used to dampen combustion instabilities. These are usually lined across the combustion chamber near the injector. They act as Helmholtz resonators and remove energy from the pressure oscillations. The cavities are sized to a certain length to tune it to the predicted frequency at which the instability manifests. Although they generally extend outwards from the chamber, a variant called a “dog-leg” which bends upward and forms an “L” shape has been used as well. Studies have shown that dog-leg cavities are more effective than straight cavities [26] [14]. Thus, dog-leg cavities will be used in the injector. A cross section of the injector dog leg cavity is shown in Figure 6.12.

A total of 15 acoustic cavity blocks will be placed inside the injector to adjust the cavity length. These are shown in Figure 6.13. These cavity blocks will be removable and exchangeable to allow testing of the engine stability margin. These will be attached via a screw from the top of the injector. Instability frequencies are dependent on the chamber temperature conditions near the cavities, so precise cavity tuning/sizing will be conducted once estimates of these temperatures are obtained.

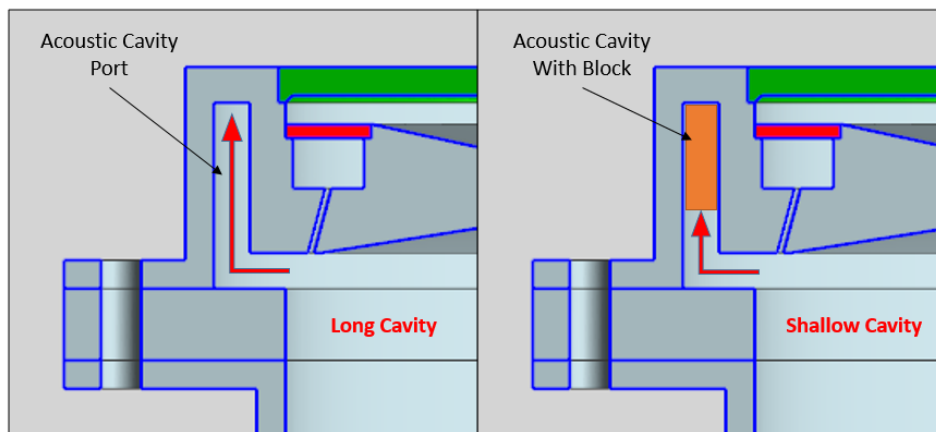


Figure 6.12: Dog-leg Cavities With and Without Acoustic Cavity Blocks

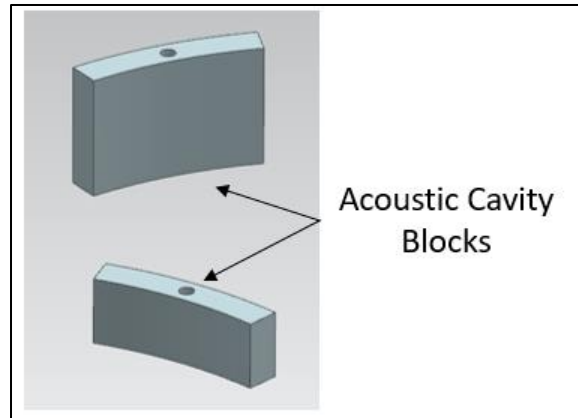


Figure 6.13: Acoustic Cavity Blocks of Different Size

Chapter 7: Engine Assembly & Inlet Propellant Requirements

Aside from the combustor and injector, a rocket engine is made up of a propellant delivery system and the vehicle interface. The delivery system of a rocket engine comprises all fluid components that deliver propellant to the engine. These components include the delivery lines, valves, instrumentation, etc. The vehicle interface is the structure that holds the engine and transmits thrust to the vehicle. These subsystems are necessary to complete the full engine configuration. The following sections describe the process to describe mentioned systems, along with the engine inlet propellant requirements.

7.1 PROPELLANT LINES ASSEMBLY, FEATURES, & INSTRUMENTATION

As described before, the engine injector has different propellant inlets. These inlets include the main combustion flow (LOX & LCH₄), the FFC, and the igniter propellant inlets. As a result, several manifolds had to be designed and sized. The criteria to size these components was the allowable pressure loss, allowable space, and orderly configuration.

The main propellant line was first defined. Initially it was decreed that the LCH₄ combustion flow rate and the FFC would have once common inlet. This was done to have a compact design and reduce the amount of connection ports to the vehicle. To size them, the velocity pressure head was compared for different line sizes. The velocity head for internal flow can be calculated using Eqn. 7.1.

$$H_{vel} = \frac{2.238\dot{w}^2}{\rho A^2} \quad (7.1)$$

Here the H_{vel} value stands for the velocity head (psi), \dot{w} is the total oxidizer or fuel weight flow rate (lbf/s), ρ is the density of the oxidizer or fuel (lbm/ft³), and A is the cross sectional area of the line [5]. Fluid mechanics dictate that a higher velocity head will lead to higher pressure losses throughout the line [20]. As a rule of thumb, the velocity head should be a small percentage of the total pressure (static and dynamic). This percentage should be around 1 – 3% [5]. Several line sizes were compared using the maximum weight flow rate of the engine and the maximum pressure upstream of the injector to obtain a velocity head pressure percentage. It was determined

that a 1" OD (0.87" ID) line would suffice, since the percentage of velocity head to total pressure is about 1.06% for LOX and about 0.8% for the total LCH₄ flow rates.

Because the methane flow rate has to split into the main LCH₄ combustion line and the FFC line, the line was branched and the size was reduced to accommodate for better inlet arrangement. The same process to determine the velocity head percentage was carried out to determine the manifold size for this branch lines. Since the pintle post was already sized to be 0.75", the combustion LCH₄ branch was reduced to a line size of 0.75" OD (0.065" ID). The FFC was reduced to 0.5" OD (0.049" ID). This resulted in a velocity head pressure percentage of 1.53% for LCH₄ combustion flow and a 1.59% for the FFC flow. Therefore the sizes were deemed acceptable. Since the engine will be tested for optimum operating parameters, it is of interest to be able to control the FFC. Thus, a valve was allocated to be in the FFC propellant branch. This valve will serve as a restriction for the FFC ports and reduce the flow. When the engine is tested, the valve will be closed gradually for each test to determine the minimum necessary cooling for steady state operation.

To ensure engine, valves, and vehicle fitting compatibility, the same type of tube fitting will be used. The fittings will be quick-clamp sanitary tube fittings (Figure 7.1). These fittings use a clamp to connect the fitting flange, conveniently allowing easy assembly. The fittings can be welded to standard tube sizes. They are rated for cryogenic use, use PTFE seals, and withstand pressures up to 1500 psi, making them compatible with the propellants. Moreover, they have been used successfully with other LOX/LCH₄ engines [14] [13].

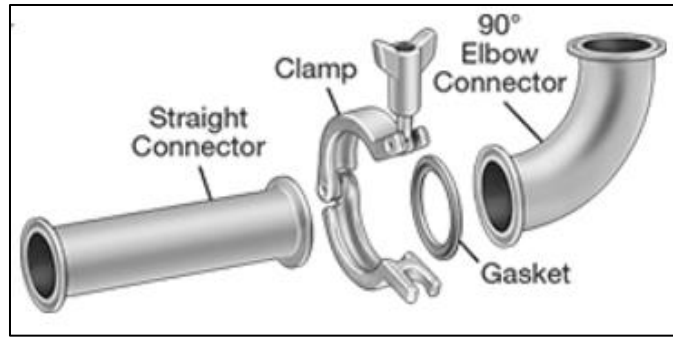


Figure 7.1: Quick-Clamp Sanitary Tube Fittings and Components [27]

The assembly of the propellant feedline is shown in Figure 7.2 and Figure 7.3. The mentioned line sizes are used, including the sanitary fittings. The assembly allows the propellant feed lines from the vehicle to be oriented in the same direction. Although the propellant lines are not entirely centered, the misalignment was deemed negligible. All lines sizes can withstand the operating pressures by a magnitude factor of safety, and all tube and fitting components are made with stainless steel 316.

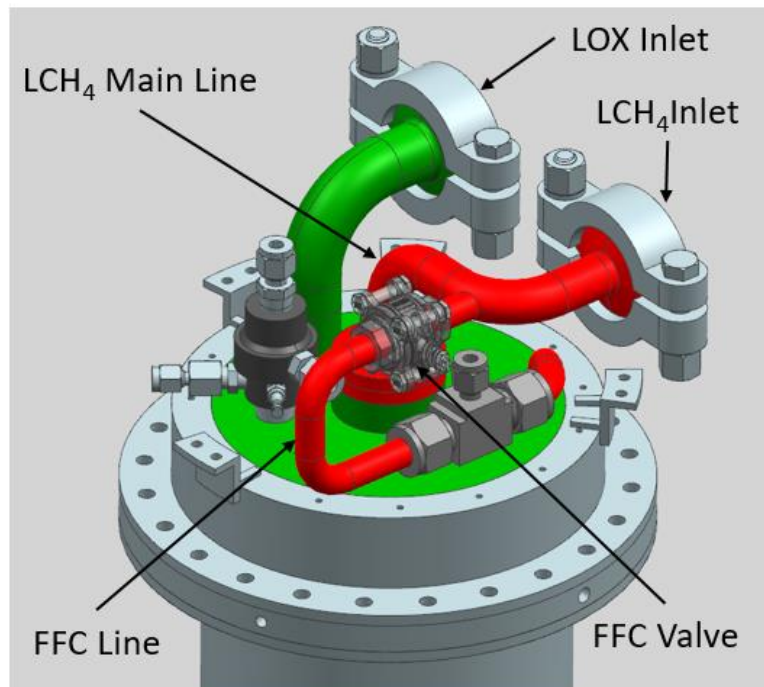


Figure 7.2: Propellant Feed Line Assembly

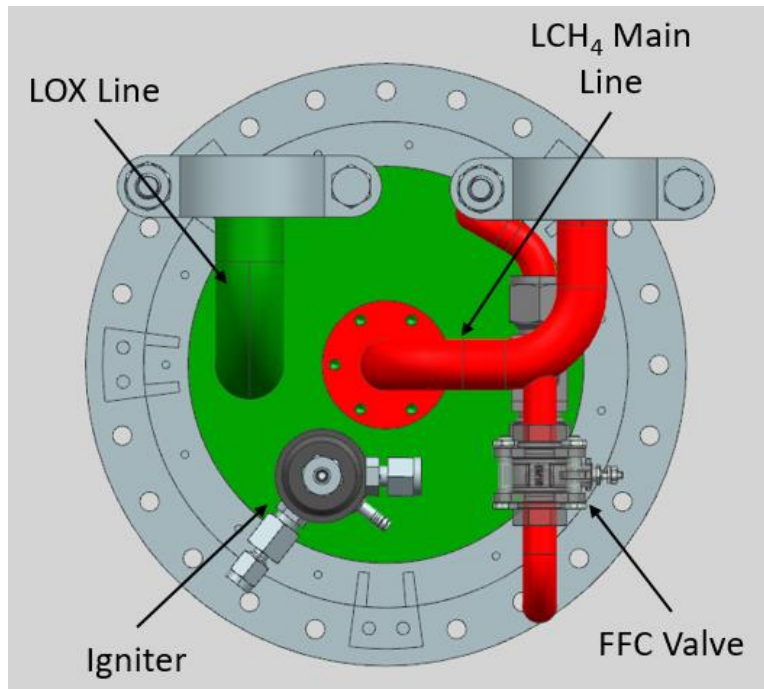


Figure 7.3: Propellant Feed Line Assembly Top View

In addition, the engine includes an instrument stand that sits on top of the injector (Figure 7.4). This stand houses two igniter propellant valves and a LOX chill by-pass valve. The igniter valves will connect directly to the vehicle delivery line. The purpose of the LOX chill by-pass is to allow LOX into the injector and chamber without opening the main LOX valve. This will allow a small LOX flow into the injector to pre-chill before a test. LOX is used to pre-chill because it is colder and less of a fire hazard when compared to LCH₄. This operation has been carried out before with similar engines [14]. The instrument stand also includes cryogenic pressure transducers (PTs) that will be connected to the propellant delivery line. A P&ID of the engine and the delivery system can be found in the Appendix.

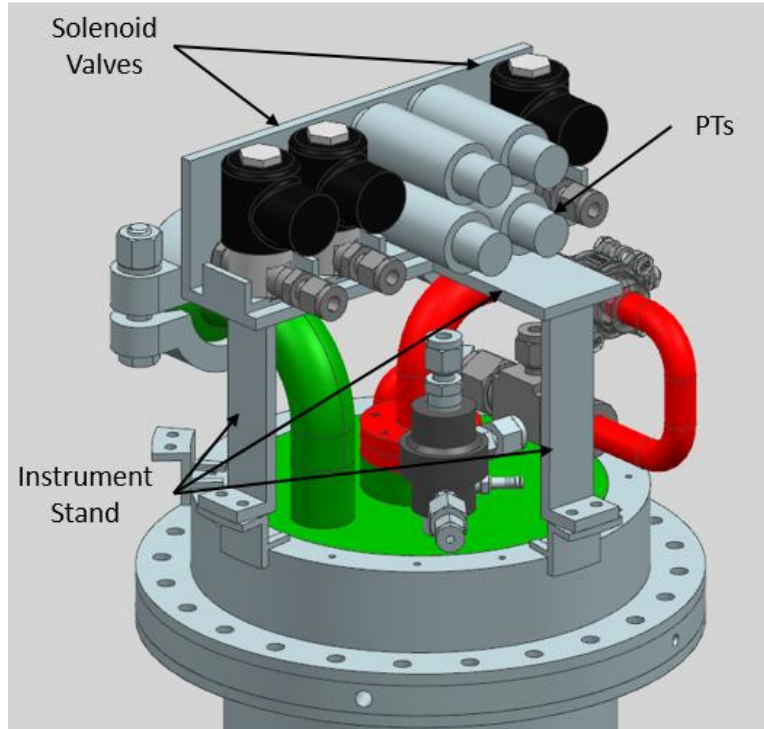


Figure 7.4: Injector Instrument Stand

To measure chamber pressure and frequency instabilities, an instrumentation ring has been included between the injector and the chamber. This ring will house the necessary instruments to measure mentioned properties. It was created as a separate component from the injector and the chamber to allow modification of the instruments that will be used, if necessary. The instrumentation ring will be made with Inconel 718 to match the combustion chamber. The first version of the instrumentation ring will hold a total of 3 high-speed pressure transducers and one static pressure transducer. Three high-speed PTs are needed to capture all the possible high-frequency instability waveforms that can be present in the engine. These need to be aligned in a 0-90-120° circular arrangement [1] [14]. The static PT will be used to measure P_c . A picture of the instrumentation ring is shown in Figure 7.5.

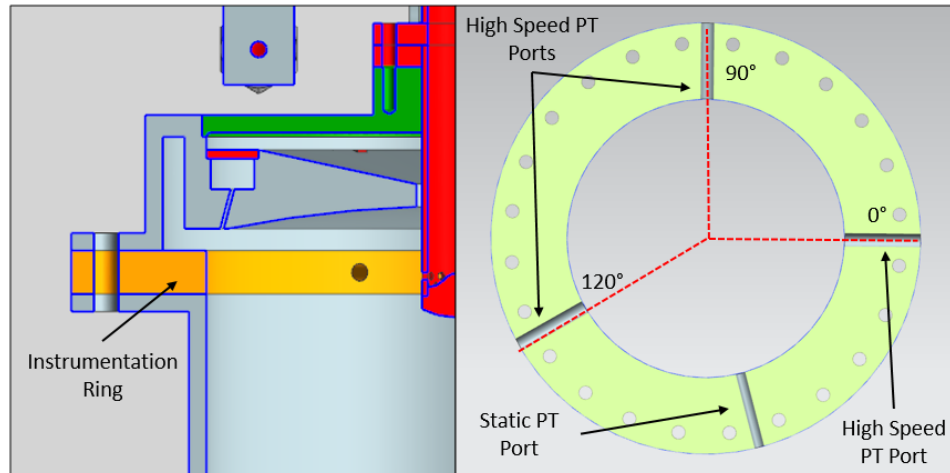


Figure 7.5: Instrumentation Ring Location & Cross Section View

7.2 VALVES & ACTUATOR ASSEMBLY

Careful consideration was taken when selecting the main engine valves. Because the valves are the throttle method for the engine, the need for a valve that offers good propellant flow control is necessary. Moreover, the valve actuator needs to allow precise and rapid control of the valve. The vehicle dynamic control depends on the thrust response. Because combustion is a fast process, the engine throttle rate is mostly dependent on valve actuation speed [4]. Therefore a rapid actuation time is required for fast control of flow rate (i.e. thrust). The valve was selected first, and then the actuator was chosen to meet the valve requirements.

7.2.1 Valve selection

The valve requirements are shown in Table 7.1. The low temperature limit ensures that any of the cryogenics are compatible with the valve. The max pressure is the same as the vehicle tanks, and the flow rates are based on the expected engine required flow rates. The max pressure drop was selected at 5 psi to minimize loss through the valve, and a 1" valve would better fit the 1" propellant line size.

Table 7.1: Main Engine Valve Requirements

Requirement	Value
Low Temperature Operating Limit	$\leq -320\text{ }^{\circ}\text{F}$
Max Operating Pressure	400 psig
Propellant Compatibility	LOX/LCH ₄
Propellant Flow Rate	LOX: 6 – 2 lb/s LCH ₄ : 3.2 – 1 lb/s
Max Pressure Drop (at max flow rate)	$\leq 5\text{ psi}$ (fully open valve)
Valve size	$\geq 1''$

Different valve types were considered for the engine. After comparing different valves available, a ball valve was selected. Compared to other valve types, ball valves require small actuation distance (a 90° actuation turn), and their simple geometry offers low pressure drop and makes them less expensive [5]. Unfortunately, standard ball valves have a non-linear response to flow due to their circular bore. As the valve is opened, a sudden large bore cross sectional area is exposed and a large flow goes through the valve. Opportunely, a variant called a “v” port valve is available for linear flow control. This valve has a “v” shape bore that is exposed more linearly as the valve is opened. This valve configuration is usually available in 30, 60, and 90° bore angles [28]. A comparison of these valves is shown in Figure 7.6.



Figure 7.6: Ball Valve V-ports vs. Round Port (30°, 60°, 90° and round port)

The minimum required flow coefficient (C_v) was obtained from the valve requirements. The C_v is a valve indicator of performance and permits valve comparison. The larger a C_v value is, the smaller the pressure drop that is caused by the valve. The equation for C_v is shown below.

$$C_v = Q \sqrt{\frac{SG}{\Delta P_v}} \quad (7.2)$$

Here, the Q value stands for the volumetric flow rate through the valve (gallons/min), SG is the specific gravity of the fluid, and ΔP_v is the pressure drop across the valve [20]. Based on the valve requirements, the minimum C_v value necessary was obtained using the max pressure drop allowed (5 psi) and the max flow rate for both propellants. It was determined that the valve would require a minimum C_v of ≈ 15 . Valve manufacturers normally report the C_v value vs. percentage openness of the valve. Several vendors were contacted to find a valve that would match for the specified requirements. It was found that the 1" 30° v-port valves normally had a C_v lower than 15, and the 1" 90° v-port valves did not yield very linear flow control. Therefore, the valve selected was the 47 series 60° v-port control valve from Habonim Industrial Valve & Actuators. This valve is 1" and has a C_v of 15.7. The body is stainless steel, making it compatible with the line size and propellants. Two valves were procured, and are shown in Figure 7.7. It can be seen that sanitary fittings were welded to the inlets.

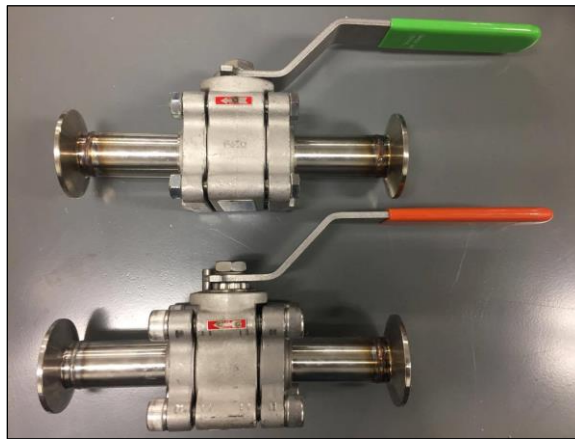


Figure 7.7: Main Engine Valves – 60° V-port Control Valve

7.2.2 Actuator selection

The actuator requirements were defined once the valve selection was made. The valve manufacturer provided break-out torque necessary to open the valve. Furthermore, the vehicle defined an actuator speed requirement and thrust resolution. These values are shown in Table 7.2.

Table 7.2: Valve Actuator Requirements

Requirement	Value
Valve Break-out Torque	187 lbf-in
Actuator Speed	0.5 seconds (fully open)
Actuator # of Positions	≥ 256 positions

The thrust resolution is defined to have 256 steps to allow subdividing the thrust range of 2000 – 500 lbf in intervals of at least ≈ 6 lbf. For a quarter turn actuation, fully opening in 0.5 seconds is the equivalent of an average speed of 30 RPM. Thus, the actuator selected would need to at least provide 187 lbf-in at 30 RPM. A DC motor from Maxxon Motors was chosen due to its capability to provide up to 42 RPM and 255 lbf-in. The motor operates at 36 VDC and 7.5 Amps, which is within the vehicle power bus capabilities. The actuator assembly includes the DC motor along with a gearbox to increase the torque output to the levels mentioned. Furthermore, it includes an encoder to program the actuator and is capable of more than 256 steps. The motor and gearbox are shown in Figure 7.8.



Figure 7.8: Actuator DC Motor (left) and Gearbox (right)

7.2.3 V-A Connector Design

To ensure compatibility between the valve and the actuator assembly, a valve-actuator (V-A) connector was designed to fit both components together. The connector purpose is to transfer the torque from the actuator to the valve, and to serve as a thermal standoff to the actuator. The actuator has a low temperature operational limit of -22°F . The valves will operate at the propellant cryogenic temperatures (down to -300°F), so the V-A connector serves as a thermal insulator.

A picture of the V-A connector is shown in Figure 7.9. The top and bottom holes are designed to fit the keyed shaft of both the valve and the actuator. The center of the connector was left hollow and surface orifices were added to ensure that the connector would have high thermal resistance. Furthermore, the V-A connector was 3D printed using the titanium alloy Ti-64. The part was 3D printed to simplify manufacturing, and titanium was used because of its high strength and relatively low thermal conductivity. A thermal and FEA analysis were conducted to ensure that the thermal gradient between the valve and the actuator would keep the actuator above -22°F . A sample temperature contour is also shown in Figure 7.9. Most results proved the V-A connector produced an acceptable thermal gradient [28]. Testing with LN2 (temperature $\approx -320^{\circ}\text{F}$) will be carried out to validate the analysis results. An assembly of the actuator, V-A connector, and valve are shown in Figure 7.10.

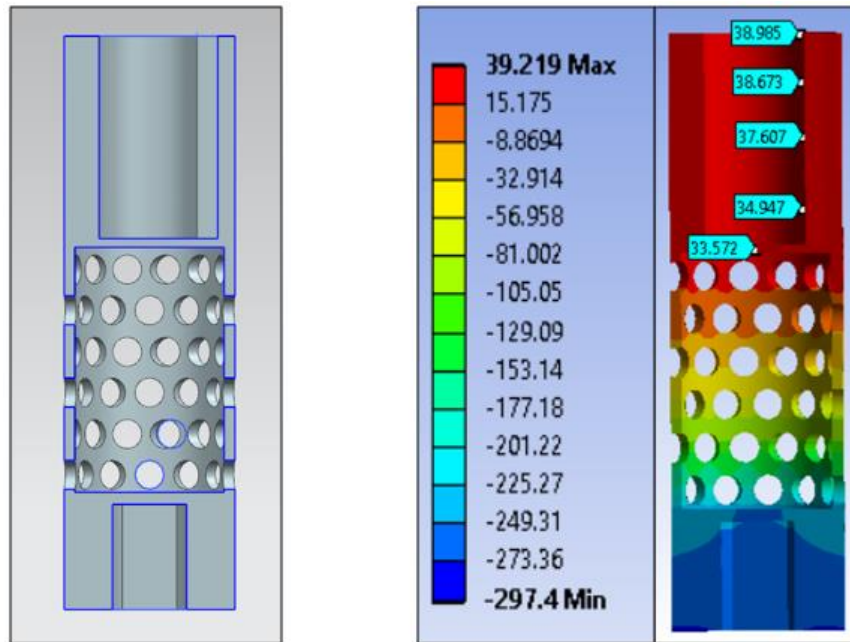


Figure 7.9: V-A Connector & Thermal Contour for Expected Thermal Gradient

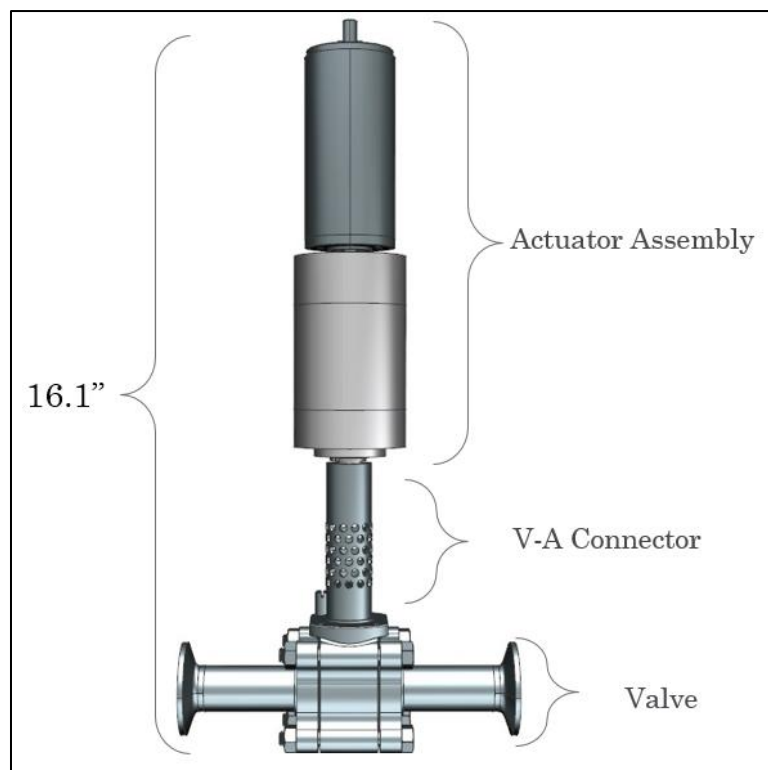


Figure 7.10: Valve-Actuator Assembly

7.3 INLET PROPELLANT REQUIREMENTS

To ensure the propellants remained liquid from the engine inlet to the point of injection, a saturation temperature and pressure analysis was conducted. The propellants will decrease in pressure as they travel the engine passages. When the static pressure of a fluid drops, so does its saturation temperature [29]. For a cryogenic propellant, this means that as the pressure drops the propellant will need to be colder for it to remain liquid. This is inconvenient because the engine has no external cold source and will only be as cold as the propellant (i.e. the propellant will readily vaporize). Therefore, introducing the propellants into the engine at the right pressure and temperature is necessary to ensure they stay in liquid phase.

To do this, the injection state of the propellants was first defined. The saturation conditions of both LOX and LCH₄ for different thrust levels are shown in Table 7.3. The pressure shown is the required chamber pressure to maintain that thrust. Hence, the temperature of the propellant has to be less than the saturation temperature (T_{sat}) at that operating pressure

Table 7.3: Propellant Required Conditions Downstream of Injection

Parameter at Injection	LOX	LCH ₄
$P_c @ F = 2000 \text{ lbf}$	232.8 psia	232.8 psia
$T_{sat} @ F = 2000 \text{ lbf}$	-228.7 °F	-171.3 °F
$P_c @ F = 500 \text{ lbf}$	75.14 psia	75.14 psia
$T_{sat} @ F = 500 \text{ lbf}$	-262.9 °F	-214.9°F
P_a	12.8 psia	12.8 psia
$T_{sat} @ P_a$	-300 °F	-259 °F

It is appreciable that at lower thrust, the lower chamber pressure has a lower saturation temperature. Thus, if the engine is to be throttled, the propellants have to be injected at a temperature $\leq -262.9 \text{ °F}$ & -214.9°F for LOX & LCH₄, respectively. This value becomes the temperature driver for the propellants. Even if the engine feed lines are well insulated, there will be an inevitable temperature gain in the propellant. Thus, a temperature margin is added to the min

temperature. A 10°F margin was subtracted to the LOX and from the LCH₄ to improve the chances of keeping a liquid propellant. It is worthy to note that at ambient pressure the propellants will be at their coldest. Thus, any temperature ranging from the saturation temperature at ambient to the margin temperature for injection will satisfy the temperature inlet conditions.

To determine the minimum inlet pressure, a pressure loss analysis was conducted to determine how much pressure loss there is throughout the propellant line. Because the valves throttle the engine, the pressure decrease required to decrease thrust will be satisfied by the valve restriction. The valve pressure loss while throttling is not an intrinsic system loss, so throttling losses are ignored in this analysis. Hence, the pressure losses considered are only the ones that inevitably reduce the propellant pressure. These were calculated at maximum flow rate and a fully open valve.

To maintain a certain thrust level, a certain pressure must be supplied upstream of the injector. The maximum pressure required before the injection orifices (P_{inj}) is equal to the sum of the max P_c and the max ΔP_{inj} at full thrust. Using the values for injector pressure drop calculated in previous sections, the max pressure required before injection is 302.7 psia. The next step is to determine the pressure loss throughout the line upstream of the injection orifices and the inlet of the valves. To do this, the following relationship was used for internal pipe flow (Eqn. 7.3) [20].

$$P_{loss} = \left(\frac{fL}{D} + \sum K \right) \frac{v^2 \rho}{2} \quad (7.3)$$

Here f stands for the Darcy-Weisbach friction factor, L is the total length of the pipe, D is the internal pipe diameter, $\sum K$ is the sum of all the minor losses in the line, v is the average fluid velocity inside pipe, and ρ is the fluid density. For turbulent flow, the friction factor is a function of Reynolds number, pipe roughness, and internal pipe diameter. This value can be obtained using a Moody chart, available in most fluid mechanics books. After ensuring that the flow is fully turbulent throughout the propellant feed line, a friction factor was obtained. The f value is between .013 - .015 for both the LOX and LCH₄ manifold. Next, the sum of the minor losses was added for each propellant delivery line. These losses include any geometry change that disrupts the flow, like

bends, fittings, contractions, etc. Using tables for different losses in pipe flow, it was determined that the $\sum K$ values are about 1.38 and 1.13 for LOX and LOX and LCH₄, respectively [20]. Lastly, by considering height changes as negligible, the change in static pressure was calculated from the Bernoulli equation (Eqn. 7.4). This equation was used to account for the changes in dynamic pressure that would occur with any enlargement or contractions in the delivery line [20]. In this equation the subscript 1 indicates the upstream conditions, and subscript 2 is the downstream conditions at any point in the line.

$$P_1 + \frac{1}{2}\rho v_1^2 = P_2 + \frac{1}{2}\rho v_2^2 + P_{loss} \quad (7.4)$$

Next, the pressure drop across the valve was calculated. Using Eqn. 7.2 along with the maximum flow rates and a $C_v = 15.7$ (fully open valve) yields a valve pressure drop of 6.6 and 5.0 psia for LOX and LCH₄. Lastly, all the pressure losses computed are shown in Table 7.4. This table also shows the necessary pressure upstream of the injection orifice.

Table 7.4: Overview of the Propellant Delivery Line Losses

Parameter	LOX	LCH ₄
Pressure upstream of Injector	302.7 psia	302.7 psia
Line losses	4.4 psi	11.5 psi
Main Valve Loss	6.6 psi	5 psi
Total P needed	313.7 psia	319.7

This table demonstrates that the greatest losses will occur in the LCH₄ line. This is caused by numerous minor losses and sudden contractions in the LCH₄ propellant line. To keep both propellant inlets requirements equivalent, the necessary LCH₄ pressure is used for both propellant lines. Adding a 2 psi margin, the required inlet pressure for both propellants was set at ≥ 322 psia. A summary of the necessary temperature and propellant conditions for both propellants is shown in Table 7.5.

Table 7.5: Engine Required Inlet Propellant Conditions

Propellant	Required Conditions
LOX	P: ≥ 322 psia Temp: -300 to -273 °F
LCH4	P: ≥ 322 psia Temp: -260 to -225°F

7.4 OVERALL ENGINE ASSEMBLY & VEHICLE INTERFACE

The full engine assembly is shown in Figure 7.11. This gives a better idea of the full engine configuration and dimensions. As can be seen, the engine envelope is within the dimensional constraints imposed by the vehicle. The current concept for vehicle interface is shown in Figure 7.12. The engine will be upheld by a structure that connects to the injector-chamber flange. The flange and the interface structure will be bolted together upon assembly. The interface structure connects to the vehicle through its outer ring by a series of bolts as well. Currently, the vehicle is at its first phase of development (called J1). This will be a static structure that will include a load cell module to measure the engine thrust. The engine, interface, and load cell module are all shown in Figure 7.13.

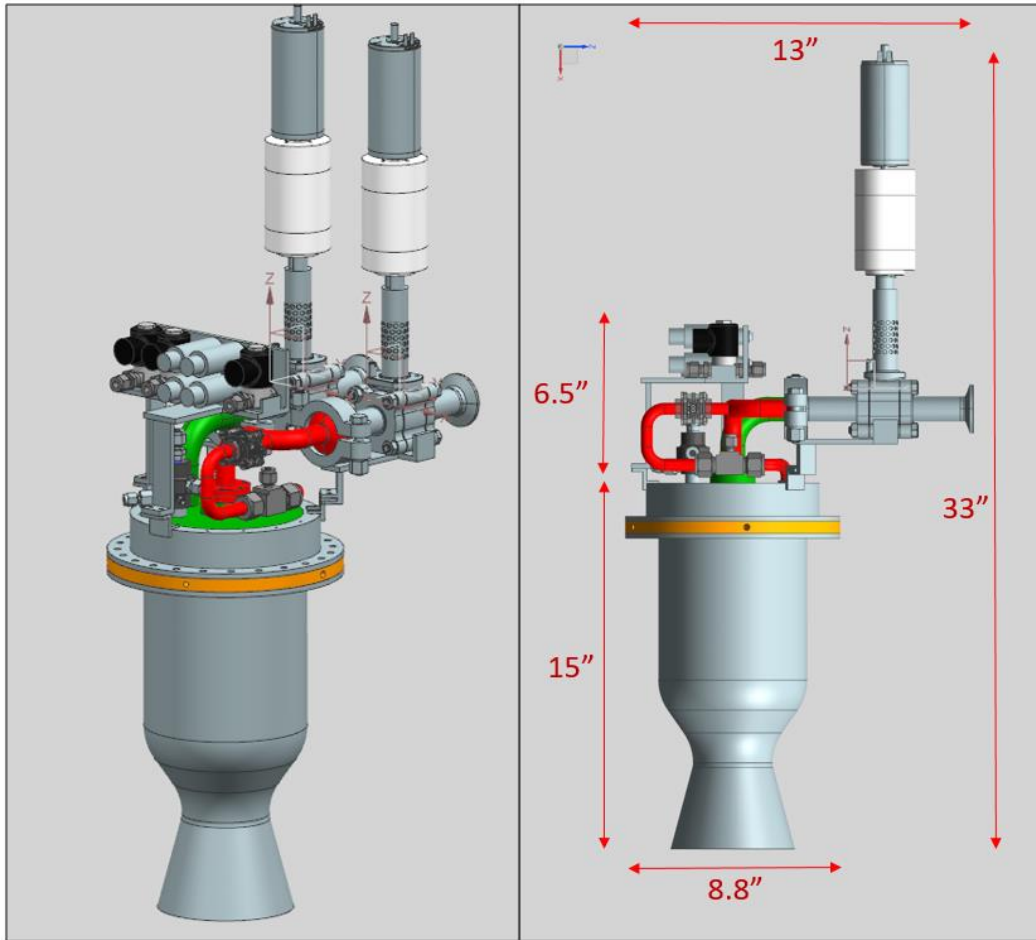


Figure 7.11: Full CROME-X Assembly and Dimensions

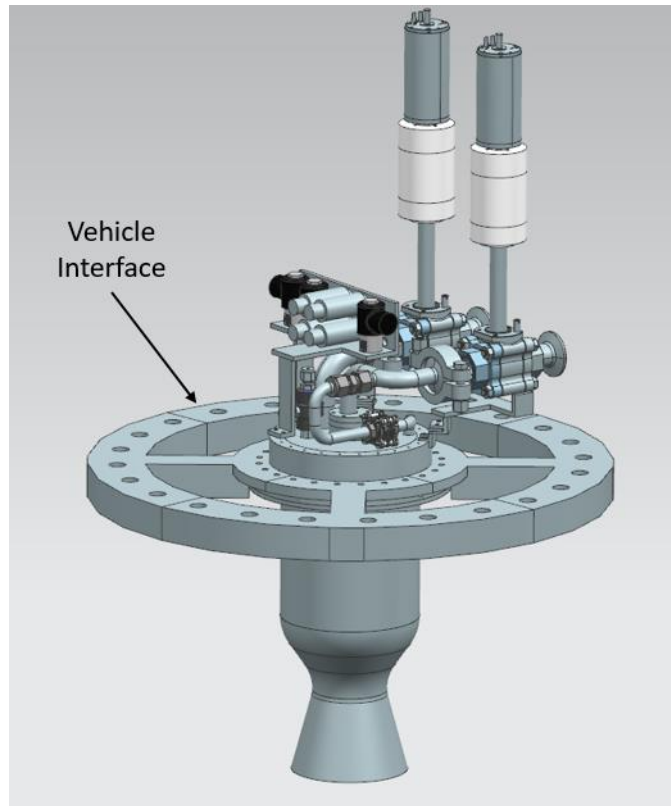


Figure 7.12: CROME-X with the Vehicle Interface

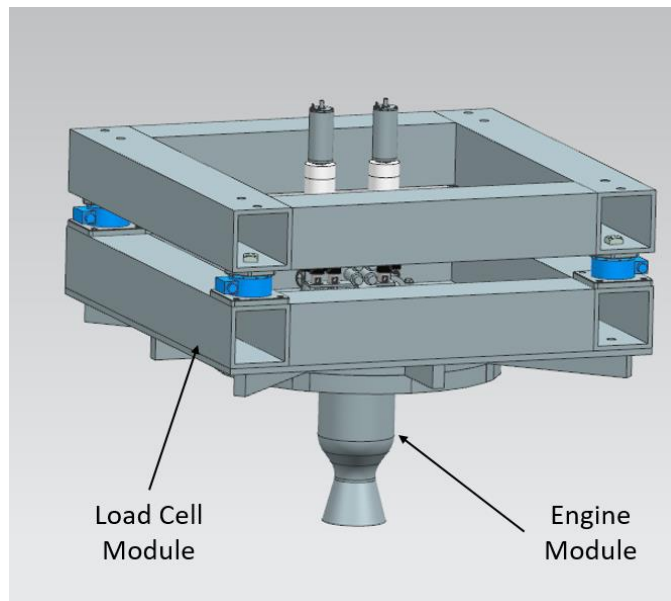


Figure 7.13: Engine Module Attached to the JANUS Load Cell Module

Chapter 8: Future Work and Conclusion

There are several tasks that need to be completed to move forward with the engine development. Different engine hardware components will be fabricated and/or procured before incorporating in the actual engine. These components will be tested beforehand to ensure acceptable operation. Moreover, other pending tasks (like design or analysis of components) will be conducted as well. Lastly, the test program for CROME-X needs to be formalized for testing at the Fabens tRIAC test site. These tasks are further discussed in the next sections.

8.1 COMPONENT TESTING & ANALYSIS

There are three hardware testing tasks that are either being conducted and/or will be conducted in the near future. These include the testing of the propellant seals, the valve & actuators tests, and injector water tests. Moreover, pending analysis on several components needs to be performed to proceed with the engine fabrication. These tasks are summarized below.

8.1.1 Propellant seal tests

Previous chapters mentioned that some component interfaces will use a PTFE sealant called GORE seal. The two interfaces are the pintle post flange and the injector-chamber flange (Figure 8.1), and these will be subject to different operating conditions. The pintle flange will be exposed to the cryogenic propellants upstream of injection, and the injector-chamber flange will be exposed to the hot combustion products. All sealants leak to some degree, so the GORE seal needs to be tested to ensure that it will have a minimal & acceptable leak rate at the operating pressures and temperatures. Moreover, there is concern that the creep/deformation will reduce the flange bolt preload over time. Thus, the seal will also be tested to measure the bolt preload loss over time when operating at cryogenic and hot temperatures.

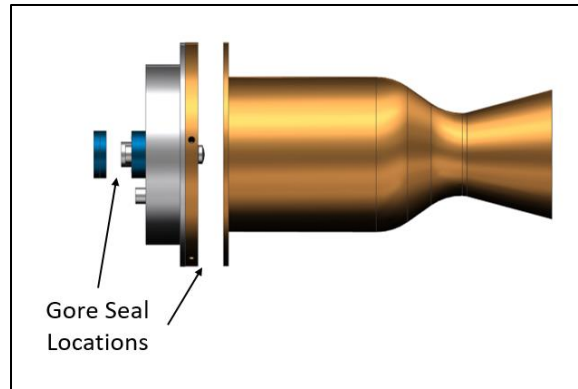


Figure 8.1: Engine Flanges That Employ Gore Seal

A flange test article was fabricated with two fluid inlets and made with similar dimensions of the injector-chamber flange (shown in Figure 8.2). The test article will be sealed to flow liquid nitrogen (LN2) and cool down to cryogenic conditions. The test article will then be filled with gaseous nitrogen (GN2) to assess the leak rate of the seal at different pressures and temperatures. Furthermore, the bolt elongation will be measured before and after testing to determine the preload loss after each test. Initial tests have already been conducted and the data is being processed. Once the cryogenic tests are finished the investigation will proceed with hot temperature conditions.

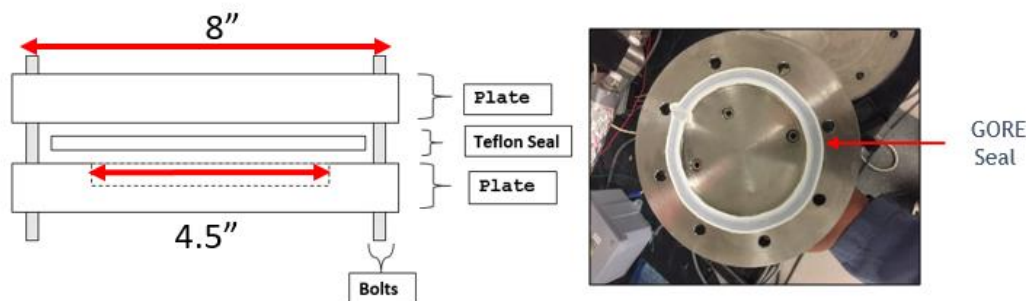


Figure 8.2: Gore Seal Test Article and Configuration

8.1.2 Valve & Actuator tests

Several aspects of the valves & actuators will be tested. First, the valves will be tested to ensure successful operation in cryogenic conditions. The valve manufacturer expressed that after prolonged use the valves can potentially leak. The valves will be tested with cryogenic flow to

mimic engine operating conditions and inspect for leaks. Second, successful actuator control will be evaluated. The actuators will be programmed and used during valve operation to ensure that they deliver the expected valve motion control. Lastly, the operating temperature of the V-A connector will be verified. The temperature of the connector will be monitored during cryogenic operation to confirm it stays within the expected temperature limits. As of now the actuators are being programmed to prepare for testing.

8.1.3 Injector water tests

Water flow tests will be carried out once the injector is manufactured to verify the injector design principles and performance. These tests will measure the actual injector pressure drop vs flowrate. These results will be compared to the theoretical expected values and the pressure drop correlations will be adjusted accordingly if necessary. Additionally, the injection stream quality will be visually examined. Specifically, the spray angle will be measured and compared to the expected theoretical angle, and the jet breakup length will be evaluated. These tests will be conducted in a water test setup that uses a pump to deliver water to the injector. The injector will eject the water into a capture container with acrylic windows to allow visual inspections of the spray. This setup has been built and will be used once the injectors are fabricated. A CAD picture of the setup is shown on Figure 8.3.

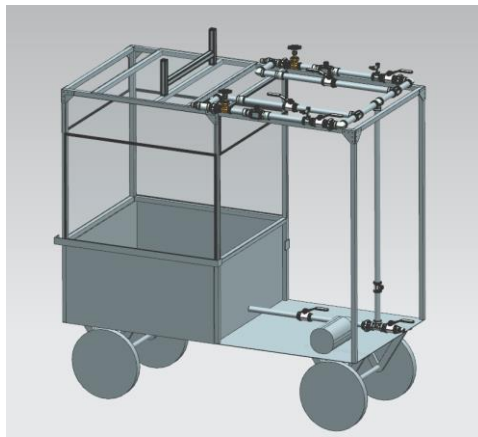


Figure 8.3: Injector Water Test Setup.

8.1.4 Pending Design & Analysis

There are a number of design related tasks that need to be done. For example, the current vehicle interface is a preliminary concept and needs to be fully defined. This component has to be completed before testing is possible. Also, an in-depth analysis of the acoustic cavity blocks is necessary to ensure engine safety. Several configurations need to be formulated to anticipate possible instability modes. Lastly, the structural and thermal analysis of the chamber and injector have to be conducted to validate or make adjustments to the current design. This step is necessary before full injector fabrication.

8.2 ENGINE HOT FIRE TESTING

The purpose of this project is to research the development of integrated LOX/LCH₄ systems. Therefore all engine systems need to be tested and evaluated for successful operation and performance. The ultimate goal of the engine is to perform a hot fire test the tRIAC test facility. Preliminary test plans are been created to conceptualize what tests are necessary and what features of the engine should be evaluated. Some of the desired tests are shown in the Table 8.1

Table 8.1: Preliminary Test Plan

Test #	Test	Description
1	Igniter Operation	Igniter tests to ensure reliable ignition
2	MR Sweep-through	Short duration tests (≤ 5 sec) with increasing MR (from low to nominal MR) to determine the MR at which ignition occurs
3	Burn Time Increase	Gradual burn time increase at nominal MR to determine if steady-state conditions are met (from 5 sec up to 40 sec)
4	Thrust Step Throttle	Steady thrust tests at different thrust levels to determine performance at a given thrust output
5	Active Throttle	Active throttle tests to evaluate successful throttle during firing through the full thrust range
6	FFC Optimization	FFC optimization tests to find the minimum FFC necessary for a given thrust level at steady state operation
7	Vehicle Flight Profile	Vehicle thrust profile tests that simulate JANUS' flight profile

8.3 OVERALL CONCLUSIONS

CROME-X is 2000 lbf rocket engine intended to be the main propulsion system for a lander vehicle called JANUS. The engine requirements included a thrust range of 2000 – 500 lbf and the use of liquid oxygen & liquid methane propellants. Design of the engine components was completed to meet those requirements. The design process for each engine component (e.g. chamber, nozzle, injector, and propellant delivery system) was described and summarized in this document. Special attention was given to the effects of throttling and how it affects engine performance. Some of the engine components will be tested to verify successful operation. Once the engine remaining analysis and design is complete, the engine will be fabricated, assembled, and undergo hot fire testing at the tRIAC test facility.

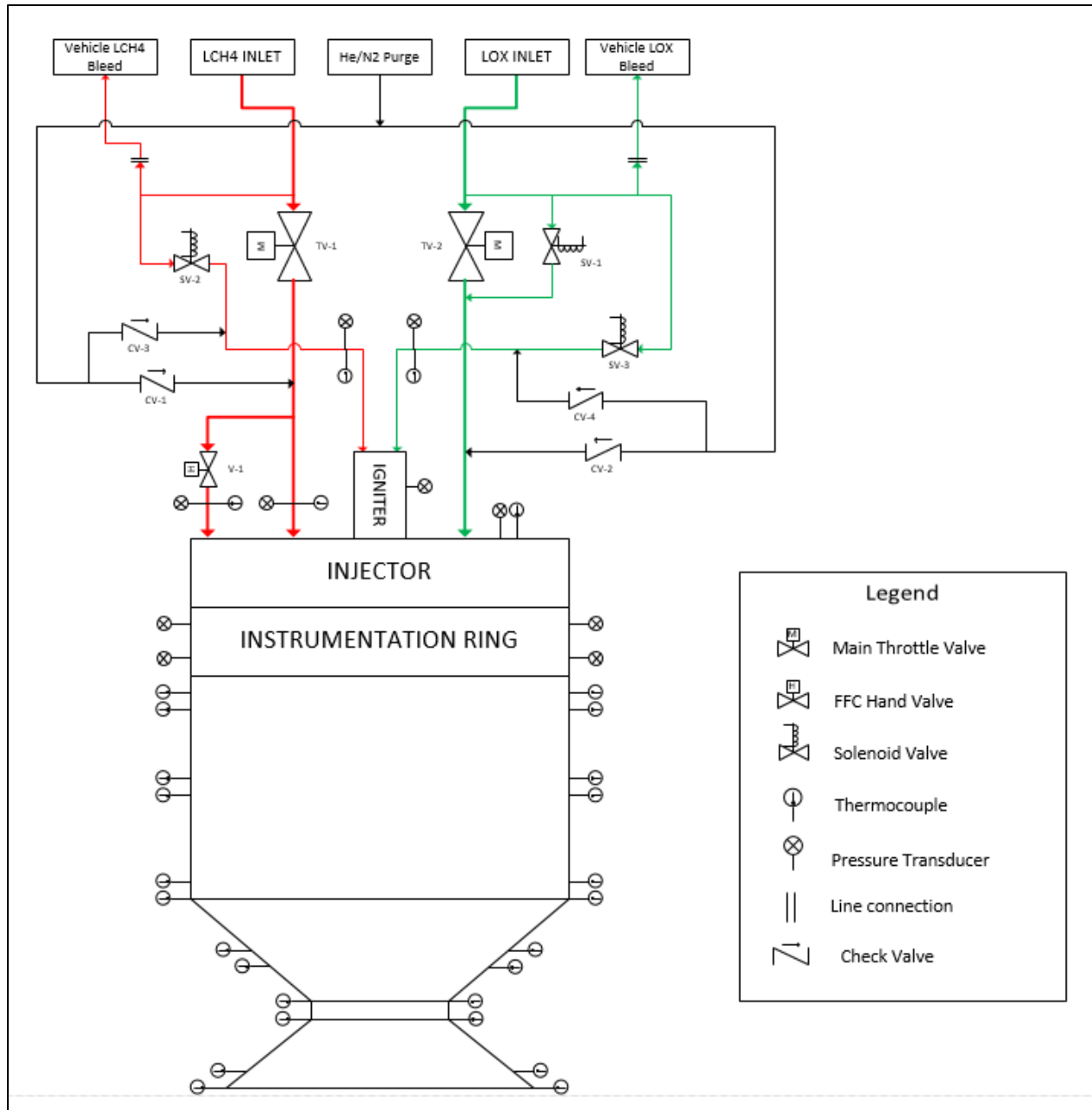
References

- [1] G. P. Sutton, *Rocket Propulsion Elements*, New York: Wiley , 2001.
- [2] D. P. Thunnissen, C. S. Guernsey, R. S. Baker and R. N. Miyake, "Advance Space Storable Propellants For Outer Planet Exploration," in *40th AIAA/ASME/SAE/ASEE Joint Propulsion Conference and Exhibit*, Fort Lauderdale, 2004.
- [3] J. B. Olansen, S. R. Munday and J. L. Devolites, "Project Morpheus: Lander Technology Development," in *AIAA SPACE 2014 Conference and Exposition* , San Diego, 2014.
- [4] C. D. Brown, *Spacecraft Propulsion*, Washington DC: American Institute of Aeronautics and Astronautics, 1996.
- [5] D. K. Huze and D. H. Huang, *Modern Engineering For Design of Liquid-Propellant Rocket Engines*, Washington DC: American Institute of Aeronautics and Astronautics, 1992.
- [6] A. A. B. J. P. C. Q. N. Shapiro, R. P. Dillon, B. McEnernery, R. Polit-Casillas and L. Soloway, "Additive Manufacturing for Aerospace Flight Applications," *JOURNAL OF SPACECRAFT AND ROCKETS*, vol. 53, no. 5, pp. 952-959, 2016.
- [7] D. M. Atyam and N. H. Nguyen, "Designing and Testing Liquid Engines for Additive Manufacturing," in *51st AIAA/SAE/ASEE Joint Propulsion Conference*, Orlando, 2015.
- [8] M. J. L. Turner, *Rocket and Spacecraft Propulsion*, New York : Springer-Verlag Berlin Heidelberg, 2009.
- [9] P. Fortescue, G. Swinerd and J. Stark, *Spacecraft System Engineering*, Chichester: John Wiley & Sons, 2011.
- [10] C. A. Snyder, "NASA Chemical Equilibrium with Applications (CEA)," NASA, 4 February 2016. [Online]. Available: <https://www.grc.nasa.gov/WWW/CEAWeb/>. [Accessed 16 September 2017].
- [11] A. Ponomarenko, "Rocket Propulsion Analysis," 2016. [Online]. Available: <http://www.propulsion-analysis.com/index.htm>. [Accessed 17 September 2016].
- [12] S. Johnson, 18 April 2013. [Online]. Available: <https://www.nist.gov/srd/refprop>. [Accessed 2 June 2016].
- [13] R. L. Morehead, "Project Morpheus Main Engine Development and Preliminary Flight Testing," in *47th AIAA/ASME/SAE/ASEE Joint Propulsion Conference & Exhibit*, San Diego, 2011.
- [14] J. C. Melcher and R. L. Morehead, "Combustion Stability Characteristics of the Project Morpheus Liquid Oxygen / Liquid Methane Main Engine," in *50th AIAA/ASME/SAE/ASEE Joint Propulsion Conference*, Cleveland, 2014.
- [15] NASA, "Safety Standard For Oxygen and Oxygen Systems," NASA, Washington DC, 1996.
- [16] Special Metals, "Inconel alloy 718," Special Metals, 2007.
- [17] Special Metals, "Inconel alloy 625," Special Metals, 2013.
- [18] W. C. Young and R. G. Budynas, *Roark's Formulas for Stress and Strain*, New York: McGraw-Hill, 2002.

- [19] G. A. Dressler and J. M. Bauer, "TRW Pintle Engine Heritage and Performance Characteristics," in *36th AIAA/ASME/SAE/ASEE Joint Propulsion Conference and Exhibit*, Las Vegas, 2000.
- [20] Y. A. Cengel and J. M. Cimbala, *Fluid Mechanics Fundamentals and Applications*, New York : McGraw-Hill, 2006.
- [21] W. E. Anderson and M. R. H. S. D. Long, "Liquid Bipropellant Injectors," in *Liquid Rocket Thrust Chambers*, West Lafayette, American Institute of Aeronautics and Astronautics, 2004, pp. 141-166.
- [22] B. L. Austin and S. D. Heister, "Characterization of Pintle Engine Performance for Nontoxic Hypergolic Bipropellant," in *38th AIAA/ASME/SAE/ASEE Joint Propulsion Conference & Exhibit*, Indianapolis, 2002.
- [23] R. D. Woodward, K. L. Miller, V. G. Bazarov, G. F. Guerin, S. Pal and R. J. Santoro, "Injector research for Shuttle OMS upgrade using LOX/ethanol propellants," in *34th AIAA/ASME/SAE/ASEE Joint Propulsion Conference and Exhibit*, Cleveland, 1998.
- [24] NASA, "Liquid Rocket engine Injectors," NASA, Springfield, 1976.
- [25] W. L. Gore & Associates, Inc, "GORE Joint Sealant for General Applications," 2017. [Online]. Available: <https://www.gore.com/products/gore-joint-sealant>. [Accessed 2 October 2016].
- [26] NASA Johnson Space Center, "2,000 lbf LOX/Methane Multi-Use Thruster CDR," 2014.
- [27] McMaster-Carr, "High-Polish Metal Quick-Clamp Sanitary Tube Fittings," 2017, [Online]. Available: <https://www.mcmaster.com/#sanitary-tube-fittings/=17k5d0j>. [Accessed 12 January 2017].
- [28] P. Nunez, L. Hernandez, I. Lopez and A. Choudhuri, "Hardware Development and Testing for a LOX/LCH₄ 2000 lbf Rocket Engine," in *The Southwest Emerging Technology Symposium 2017*, El Paso, 2017.
- [29] Y. Cengel and M. Boles, *Thermodynamics: An Engineering Approach*, New York: McGraw-Hill, 2014.

Appendix

CROME-X P&ID



Vita

Israel Lopez was born in El Paso, TX, on August 16, 1992. He was first raised in Ciudad Juarez, Mexico, and moved back to El Paso at the age of 10. He attended Bel Air High School and graduated in the spring of 2010. He then continued his education at the University of Texas at El Paso, receiving his Bachelor of Science Degree in Mechanical Engineering in the spring of 2014. During his undergraduate education, Israel began working under the supervision of Dr. Ahsan Choudhuri at the Center for Space Exploration and Technology Research (cSETR). Israel began working at cSETR during the fall of 2013 where his main focus of work comprised research on LOX/LCH₄ rocket propulsion systems. He was accepted to the Master of Science in Mechanical Engineering program where he proceeded to receive his Master's Degree the spring of 2017. During his academic career at UTEP, Israel had the opportunity to intern at Blue Origin and NASA Johnson Space Center.

Permanent address: 12133 Tower Hill Dr
El Paso, TX, 79936

This thesis/dissertation was typed by Israel Lopez